nature plants

Article

https://doi.org/10.1038/s41477-023-01477-y

The master growth regulator DELLA binding to histone H2A is essential for DELLA-mediated global transcription regulation

Received: 14 December 2022

Accepted: 4 July 2023

Published online: 3 August 2023

Check for updates

Xu Huang[1,8], Hao Tian[1,4,8], Jeongmoo Park[1,5,8], Dong-Ha Oh[2], Jianhong Hu[1], Rodolfo Zentella[1,6,7], Hong Qiao[3], Maheshi Dassanayake[2] & Tai-Ping Sun[1]

The *DELLA* genes, also known as 'Green Revolution' genes, encode conserved master growth regulators that control plant development in response to internal and environmental cues. Functioning as nuclear-localized transcription regulators, DELLAs modulate expression of target genes via direct protein–protein interaction of their carboxy-terminal GRAS domain with hundreds of transcription factors (TFs) and epigenetic regulators. However, the molecular mechanism of DELLA-mediated transcription reprogramming remains unclear. Here by characterizing new missense alleles of an *Arabidopsis DELLA*, repressor of *ga1-3* (*RGA*), and co-immunoprecipitation assays, we show that RGA binds histone H2A via the PFYRE subdomain within its GRAS domain to form a TF–RGA–H2A complex at the target chromatin. Chromatin immunoprecipitation followed by sequencing analysis further shows that this activity is essential for RGA association with its target chromatin globally. Our results indicate that, although DELLAs are recruited to target promoters by binding to TFs via the LHR1 subdomain, DELLA–H2A interaction via the PFYRE subdomain is necessary to stabilize the TF–DELLA–H2A complex at the target chromatin. This study provides insights into the two distinct key modular functions in DELLA for its genome-wide transcription regulation in plants.

The *DELLA* genes are also known as 'Green Revolution' genes because of their pivotal role in modulating stature of the high-yielding wheat varieties, which were crucial for the success of the Green Revolution in the 1960s[1–3]. The *DELLA* genes were originally identified by genetic analyses as repressors of the phytohormone gibberellin (GA) signalling in *Arabidopsis thaliana*[4,5]. Further studies showed that DELLAs are conserved in all land plants[6], and they function as pivotal integrators of multiple signalling pathways to modulate plant growth and

[1]Department of Biology, Duke University, Durham, NC, USA. [2]Department of Biological Sciences, Louisiana State University, Baton Rouge, LA, USA. [3]Institute for Cellular and Molecular Biology and Department of Molecular Biosciences, The University of Texas at Austin, Austin, TX, USA. [4]Present address: Department of Botany and Plant Sciences, University of California, Riverside, Riverside, CA, USA. [5]Present address: Syngenta, Research Triangle Park, Raleigh, NC, USA. [6]Present address: Agricultural Research Service, Plant Science Research Unit, US Department of Agriculture, Raleigh, NC, USA. [7]Present address: Department of Crop and Soil Sciences, North Carolina State University, Raleigh, NC, USA. [8]These authors contributed equally: Xu Huang, Hao Tian, Jeongmoo Parkg. e-mail: tps@duke.edu

https://doi.org/10.1038/s41477-023-01477-y

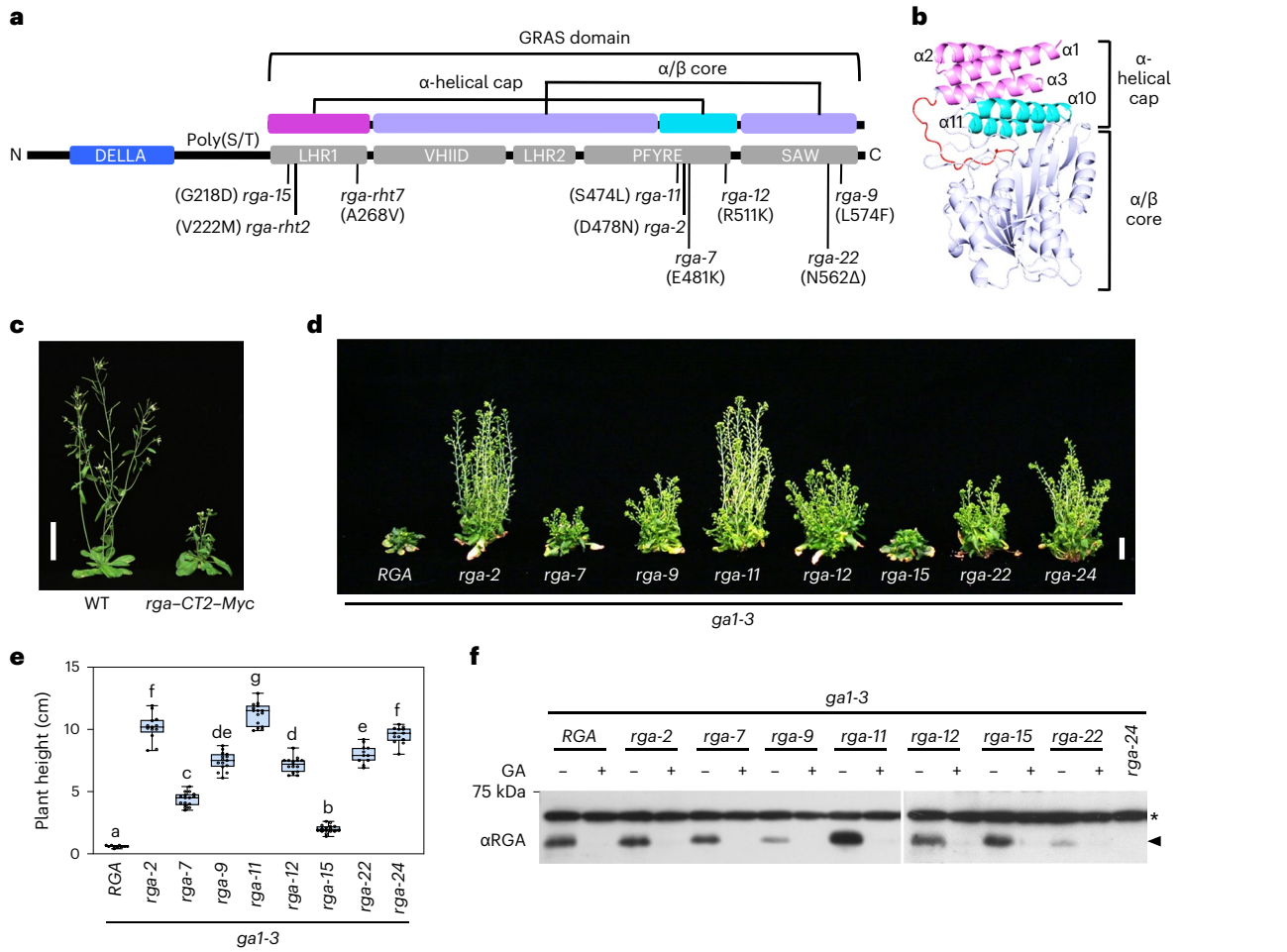

Fig. 1 | All missense *rga* hypomorphs are clustered within the GRAS domain. **a**, Domain map of the RGA protein. The missense *rga* alleles and corresponding amino acid substitutions or deletion are labelled. The two subdomains (α-helical cap and α/β core) of the GRAS domain are colour-coded as in **b**. **b**, Predicted 3D structure of RGA GRAS domain using SWISS-MODEL[50,71] with the SCARECROW protein (PDB: 5B3G)[49] as scaffold. The GRAS domain contains an α-helical cap (α1–α3 in magenta and α10–α11 in cyan), and an α/β core (in purple). **c**, Expression of P_{RGA}:*rga-CT2-Myc* (rga-CT2 containing residues 207–587 (ref. 45)) in WT *Arabidopsis* caused a semi-dwarf phenotype. Photo of representative 43-day-old plants in long-day conditions. Scale bar, 5 cm. **d**–**e**, Missense *rga* alleles displayed varying effects on rescuing *ga1* dwarf phenotype. **d**, Representative 70-day-old *ga1-3* (with *RGA*) and *ga1 rga* mutants, as labelled. Scale bar, 2 cm. **e**, Box plot showing plant heights of different lines, as labelled. $n \geq 11$. Centre lines and box edges are medians and the lower and upper quartiles, respectively. Whiskers extend to the lowest and highest data points within 1.5× interquartile range (IQR) below and above the lower and upper quartiles, respectively. Different letters above the bars represent significant differences ($P < 0.01$), as determined by two-tailed Student's *t*-tests. Exact *n* and *P* values are listed in Source Data Fig. 1. **f**, Missense rga proteins were responsive to GA-induced degradation. Immunoblot contained protein extracted from seedlings that were treated with 1 μM GA_4 (+) or mock treated (−) for 1 h. The blot was probed with an anti-RGA antiserum. * Represents non-specific background band. The arrow represents RGA protein. Representative images of two biological repeats are shown.

development in response to biotic and abiotic cues[3,7,8]. DELLAs belong to the DELLA subfamily of the plant-specific GRAS family of proteins with a conserved carboxy-terminal (C-terminal) GRAS domain that confers transcriptional regulator function (Fig. 1a)[4,5,9,10]. The unique DELLA domain in its amino terminus is required for its response to GA-induced degradation[11,12], and this domain is absent in other GRAS family members. Biochemical and structural studies showed that GA triggers a conformational switch in its receptor GID1 to promote GA–GID1–DELLA domain complex formation, which in turn enhances binding of the $SCF^{SLY1/GID2}$ E3 ubiquitin ligase to the GRAS domain for polyubiquitination and subsequent degradation by the 26S proteasome[13–18]. Chromatin immunoprecipitation–quantitative PCR (ChIP–qPCR) and subsequent chromatin immunoprecipitation followed by sequencing (ChIP-seq) analyses showed that repressor of *ga1-3* (RGA) (an At*DELLA*) is associated with its target promoters, although it does not contain a canonical DNA-binding motif[19–21]. Extensive studies indicate that DELLA proteins regulate expression of target genes by direct interaction of the GRAS domain with transcription factors (TFs) or regulators and epigenetic regulators[3,7,8]. However, the molecular mechanism of DELLA-mediated transcription reprogramming remains unclear.

Remarkably, a total of 370 potential DELLA-interacting proteins have been identified by yeast two-hybrid (Y2H) screens, and more than 40 of these have been verified with co-immunoprecipitation (co-IP) and/or genetic analyses[8,22,23]. Most of the DELLA-interacting proteins are TFs or transcription regulators. Examples of DELLA-inhibited TFs or transcription regulators include PHYTOCHROME INTERACTING FACTORs (PIFs), basic helix–loop–helix (bHLH) TFs involved in light signalling[24,25]; the auxin signalling activators AUXIN RESPONSE FACTORs (ARFs)[26,27]; BRASSINAZOLE-RESISTANT 1 (BZR1), a brassinosteriod signalling activator that contains a non-canonical bHLH domain[28]; the jasmonic acid signalling repressors JAZs[29,30]; and type I TCP (TEOSINTE BRANCHED 1 (TB1), CYCLOIDEA (CYC) and PROLIFERATING CELL FACTOR (PCF)) TFs[31]. DELLA-activated TFs or transcription regulators include type B ARABIDOPSIS RESPONSE REGULATORs

https://doi.org/10.1038/s41477-023-01477-y

in cytokinin signalling[21], ABSCISIC ACID INSENSITIVE 3 (ABI3) and ABI5 (a bZIP TF) in ABA signalling[32], and INDETERMINATE DOMAIN (IDD) subfamily of C2H2 zinc-finger TFs[33,34]. Other DELLA interactors include chromatin-remodelling complexes (SWI/SNF and a CHD protein PICKLE (PKL))[35–37], and subunits of the prefoldin complex for tubulin folding[38]. These findings indicate that protein–protein interactions with TFs or transcription regulators is a major regulatory mechanism in DELLA-modulated plant development. DELLAs function as co-activators or co-repressors, depending on their interacting TFs. The current model proposes two distinct modes of DELLA action: (1) DELLA-mediated transcription activation of target genes depends on its recruiting TFs (for example, IDDs), which bind to both DELLA and the target promoter sequences; and (2) DELLA alters transcription by blocking DNA binding and hence sequestration of transcription activators (for example, BZR1, PIFs and TCPs) or repressors (for example, JAZs) from target promoters[7,8].

Previous mutant and transgenic studies indicate that the GRAS domain is required for the growth suppression activity of DELLA proteins. Loss-of-function *della* missense mutations in several plant species are all located within the GRAS domain[4,39–42]. The GRAS domain contains five conserved subdomains: leu heptad repeat 1 (LHR1), VHIID, LHR2, PFYRE and SAW (Fig. 1a). Evidence from previous serial deletion studies by Y2H and in vitro pulldown assays suggested that LHR1 is required for protein–protein interactions with many DELLA interactors, although C-terminal truncations of other GRAS subdomains often also abolish these interactions[8]. These results cannot distinguish between specific defects in the protein interaction motif versus general defects in protein conformation and structural stability. Genetic analysis and alanine scanning mutagenesis further revealed that VHIID and LHR2 are involved in the F-box protein binding[43,44]. However, the roles of the C-terminal PFYRE and SAW regions are unclear.

To elucidate the molecular mechanism of DELLA function in transcription regulation, it is crucial to decipher the specific roles of its GRAS subdomains. In this Article, we characterized the effects of a number of missense *rga* alleles on plant growth and interaction with TFs by Y2H, pulldown and co-IP assays. Surprisingly, missense mutations in the PFYRE subdomain did not dramatically affect interaction with TFs (BZR1, PIF, TCP14 and IDD3). We further identified a function of the PFYRE subdomain for binding to histone H2A. ChIP–seq analysis showed that this activity is crucial for genome-wide RGA association with its target chromatin. Our results indicate that, although TFs are required to recruit the DELLA protein via its LHR1 subdomain to target gene promoters, DELLA–H2A interaction via its PFYRE subdomain is necessary to stabilize the H2A–DELLA–TF complex at the target chromatin site.

Results

RGA's PFYRE subdomain plays a key role in growth suppression

We directly examined the GRAS function of an At*DELLA* RGA by expression of the RGA GRAS domain under the control of an *RGA* promoter (P_{RGA}*:rga–CT2–Myc*) in transgenic *Arabidopsis*[45]. P_{RGA}*:rga–CT2–Myc* led to a semi-dwarf phenotype (Fig. 1c) that does not respond to GA treatment (Supplementary Fig. 1), supporting that the GRAS domain of DELLA alone is sufficient to confer growth suppression. Among the five conserved subdomains in the GRAS domain, LHR1 interacts with TFs[8], and VHIID and LHR2 are required for F-box protein binding[43,44]. To elucidate the specific functions of the PFYRE and SAW subdomains at the C terminus of the GRAS domain in RGA, we sequenced a large collection of *rga* mutants, which we isolated in previous *ga1-3* suppressor mutant screens (Supplementary Table 1)[4,46]. Among the 27 *rga* mutants, we found 8 nonsense *rga* mutations, which are distributed throughout the RGA coding sequence. In contrast, all single-amino-acid mutations (seven in total) are located within the GRAS domain: one missense mutation (*rga-15*) is located in LHR1, four missense mutations

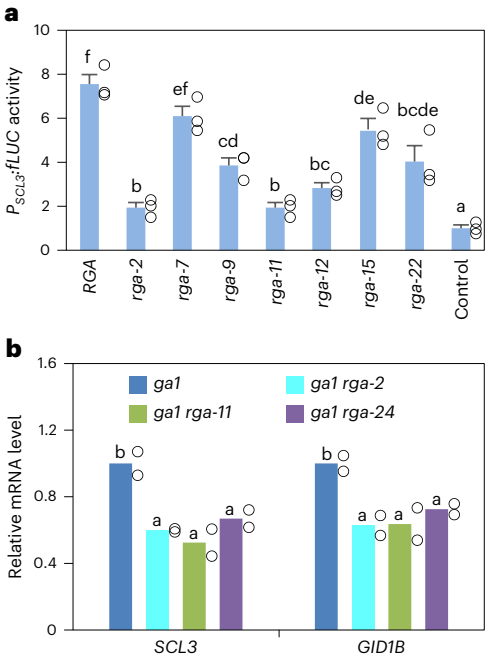

Fig. 2 | Missense rga mutant proteins showed varying degrees of reduced activity. a, Dual LUC assay in the *N. benthamiana* transient expression system showing that, compared with RGA, rga mutant proteins were impaired in activating P_{SCL3}*:fLUC*. Means ± s.e. of three biological replicates are shown. The relative P_{SCL3}*:fLUC* activity in the control sample was set to one. The reporter construct contained P_{SCL3}*:fLUC*[48]. Effector constructs contained *35S:RGA* or *rga* as labelled, and the empty vector was included as a negative control. RGA and rga proteins were expressed at similar levels in these assays (Supplementary Fig. 2a). **b**, RT-qPCR analysis showing *rga-2* and *rga-11* caused reduced expression of RGA-induced genes (*SCL3* and *GID1B*) in planta, similar to the null *rga-24* allele. The housekeeping gene, *PP2A*, was used to normalize different samples. Means of two biological replicates are shown. The level in *ga1-3* was set to one. In **a** and **b**, statistical analyses were performed with two-tailed (**a**) or one-tailed (**b**) Student's *t*-tests. Different letters above the bars represent significant differences, $P < 0.05$. Exact *n* and *P* values are listed in Source Data Fig. 2.

are clustered within PFYRE and two mutations (a deletion and a missense mutation) are in SAW (Fig. 1a and Supplementary Table 1). These mutations conferred varying degrees of suppression of the GA-deficient dwarf phenotype of *ga1-3* (Fig. 1d,e). Among them, *rga-2* and *rga-11* (PFYRE mutations) showed the strongest phenotypes that are similar to the null allele *rga-24*, suggesting that the PFYRE subdomain plays a key role in RGA function. All these rga proteins remained responsive to GA-induced degradation (Fig. 1f), indicating they are able to interact with GID1 and SLY1.

To examine the activity of these *rga* alleles on target gene expression, a dual luciferase (LUC) assay[47] was carried out using the transient expression system in *Nicotiana benthamiana*. The P_{SCL3}*:firefly LUC* (*fLUC*) was used as the reporter for this assay because *SCL3* is a direct target gene of DELLA, and its transcription is induced by DELLA[19,48]. *35S:Renilla LUC* was the internal control to normalize variations in transformation efficiency. The effectors included *35S:RGA* and *35S:rga* constructs. As expected, when co-expressed with *35S:RGA*, P_{SCL3}*:fLUC* expression was induced about eightfold compared with the negative control (with the empty effector construct) (Fig. 2a). The rga mutants showed reduced transactivation activity (Fig. 2a and Supplementary Fig. 2a), which correlated with the corresponding mutant phenotypes (Fig. 1d,e). Reverse transcription quantitative PCR (RT-qPCR) analysis further indicated that mRNA levels of RGA-induced genes (*SCL3* and *GID1B*) were reduced in *rga-2* and *rga-11*, similar to *rga-24*, compared with wild type (WT) (Fig. 2b).

https://doi.org/10.1038/s41477-023-01477-y

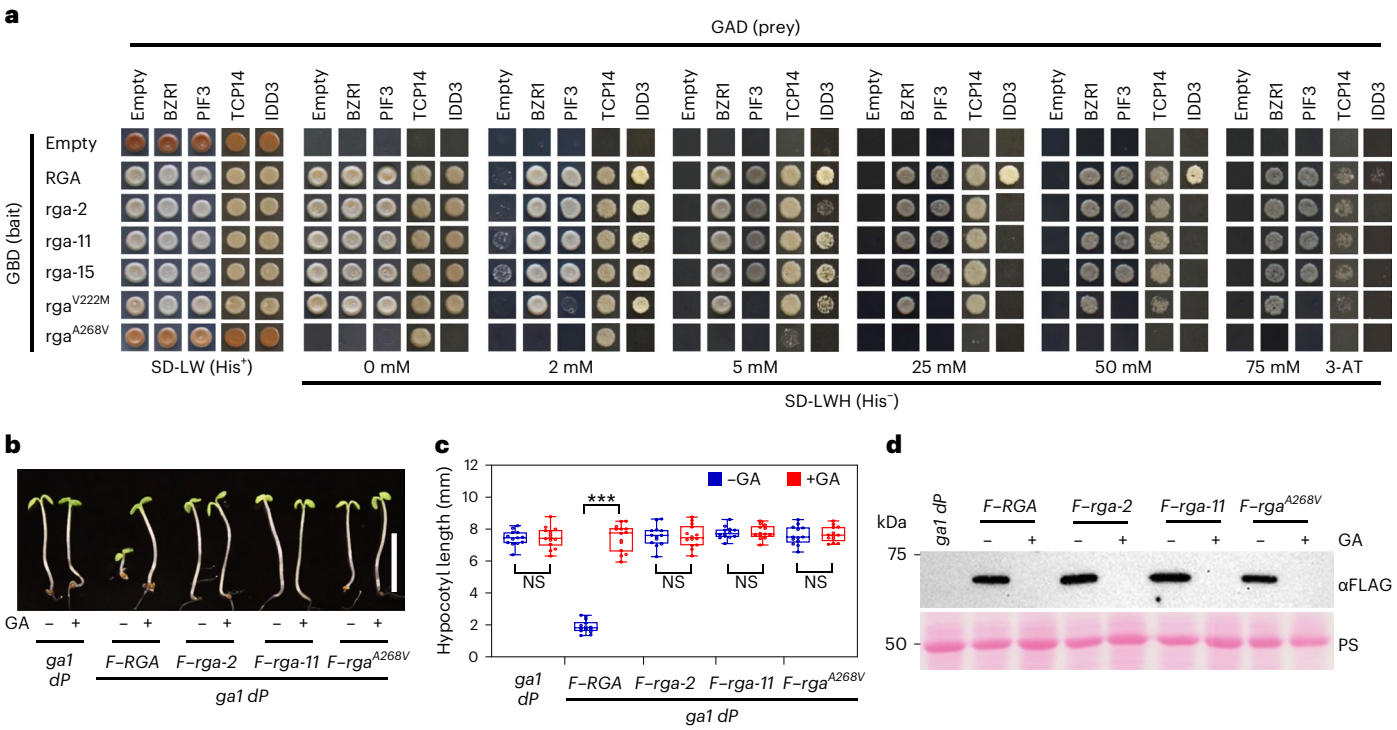

Fig. 3 | Y2H assay showed rga mutations in the LHR1 subdomain reduced interaction with BZR1, PIF3 and TCP14, whereas rga-2 and rga-11 in PFYRE did not. a, Y2H assay showing that rga-2 and rga-11 interacted with BZR1, PIF3 and TCP14 similarly to WT RGA, but rga^{V222M} reduced binding to PIF3 and rga^{A268V} abolished binding to BZR1, PIF3, TCP14 and IDD3. The bait constructs expressed truncated RGA or rga (amino acid residues 107–587) with Gal4 DNA-binding domain fusion (GBD). The prey constructs expressed TFs with Gal4 transactivation domain (GAD) as labeled. The strength of interaction was indicated by the ability of cells to grow on His$^-$ plates with 0–75 mM 3-AT (3-amino-1,2,4-triazole). SD-LW, medium lacking Leu and Trp. The lower amounts of rga-2 protein expressed in yeast cells may contribute to the reduced growth of rga-2 and IDD3 compared with other rga proteins (Supplementary Fig. 2b). Representative images of three biological repeats are shown. **b-c**, FLAG–RGA suppressed hypocotyl growth of *ga1 dP*, whereas FLAG–rga-2 and FLAG–rga-11 did not. Transgenic seedlings containing P_{RGA}*:FLAG–RGA*, *FLAG–rga-2* or *FLAG–rga-11* in the *ga1 dP* background were grown on media without (–) or with 25 μM GA_3 (+) as labelled. **b**, Representative 5-day-old seedlings in short-day conditions. Scale bar, 5 mm. **c**, Box plot showing hypocotyl lengths of different lines as labelled. $n \geq 13$. *** $P < 0.001$. Statistical analyses were performed with two-tailed Student's *t*-tests. Centre lines and box edges are medians and the lower and upper quartiles, respectively. Whiskers extend to the lowest and highest data points within 1.5× IQR below and above the lower and upper quartiles, respectively. Exact *n* and *P* values are listed in Source Data Fig. 3. **d**, The amounts of FLAG–rga proteins were similar to FLAG–RGA in these transgenic lines. Immunoblot contained protein extracts from seedlings grown as in **b**, and the blot was probed with an anti-FLAG antibody. Representative image of two biological repeats are shown. F, FLAG; NS, no significant difference; PS, Ponceau S-stained gel blot.

To understand the structure–function relationship of the DELLA GRAS domain, we generated the three-dimensional (3D) structure model of the RGA GRAS domain based on the crystal structure of another *Arabidopsis* GRAS protein, SCARECROW (SCR)[49] using the online SWISS-MODEL workspace (http://swissmodel.expasy.org/)[50] (Fig. 1b). The predicted RGA GRAS domain contains one α/β core subdomain with an α-helical cap. The α-helical cap consists of five α-helixes: α1–α3 (corresponding to LHR1) and α10–α11 (part of the PFYRE subdomain). The remaining GRAS sequence forms the α/β core. Three missense mutations (rga-2, rga-11 and rga-7) within the PFYRE subdomain of RGA are located in the predicted α10 in the α-helical cap, suggesting this region plays an important role in the growth suppression activity of RGA.

LHR1 subdomain, but not PFYRE, is required for TF binding

To investigate the molecular function of the PFYRE subdomain, we first tested whether rga-2 and rga-11 (containing PFYRE mutations) are impaired in binding to four DELLA-interacting TFs, BZR1, PIF3, TCP14 and IDD3. Surprisingly, these mutations only reduced IDD3 interaction, but did not affect binding with BZR1, PIF3 or TCP14 by Y2H assay (Fig. 3a and Supplementary Fig. 2b). To further decipher the functional defect of rga-2 and rga-11, we generated transgenic *Arabidopsis* carrying P_{RGA}*:FLAG–RGA*, *FLAG–rga-2* or *FLAG–rga-11* fusion genes, separately, in the *ga1-3 della pentuple (ga1 dP)* background. In *ga1 dP*, all five *Arabidopsis DELLA* genes (*RGA*, *GA-INSENSITIVE* (*GAI*), *RGA-LIKE1* (*RGL1*), *RGL2* and *RGL3*) were knocked out[37]. As expected, P_{RGA}*:FLAG–RGA* restored the dwarf phenotype in the *ga1 dP* background (Fig. 3b,c) because *RGA* plays a major role in repressing vegetative growth[51,52]. *FLAG–rga-2* and *FLAG–rga-11* were inactive as they did not suppress growth of *ga1 dP* (Fig. 3b,c and Supplementary Fig. 3a,b), although the FLAG–rga-2 and FLAG–rga-11 protein levels in these lines were similar to the FLAG–RGA levels in the *FLAG–RGA* line (Fig. 3d). In vitro pulldown assays were performed with recombinant GST-tagged BZR1 and PIF3 expressed in *Escherichia coli*, and protein extracts from transgenic *Arabidopsis* expressing FLAG–RGA or FLAG–rga (Fig. 4a and Supplementary Fig. 4a). Consistent with the Y2H results, FLAG–rga-2 and FLAG–rga-11 showed similar binding affinity to GST–BZR1/PIF3 as that of FLAG–RGA. GST–IDD3 was insoluble in *E. coli*. To examine the effect of rga mutations on IDD3 binding, in vitro pulldown assays were performed using recombinant maltose-binding protein (MBP)–RGA, MBP–rga-2 and MBP–rga-11 with protein extracts from *N. benthamiana* expressing FLAG–IDD3. We also included FLAG–PIF4 in this assay. MBP–rga-2 and MBP–rga-11 showed similar binding affinity to FLAG–IDD3 and FLAG–PIF4 as that of MBP–RGA (Supplementary Fig. 4b). These results strongly support that these mutations in the PFYRE subdomain do not dramatically affect RGA binding to BZR1,

https://doi.org/10.1038/s41477-023-01477-y

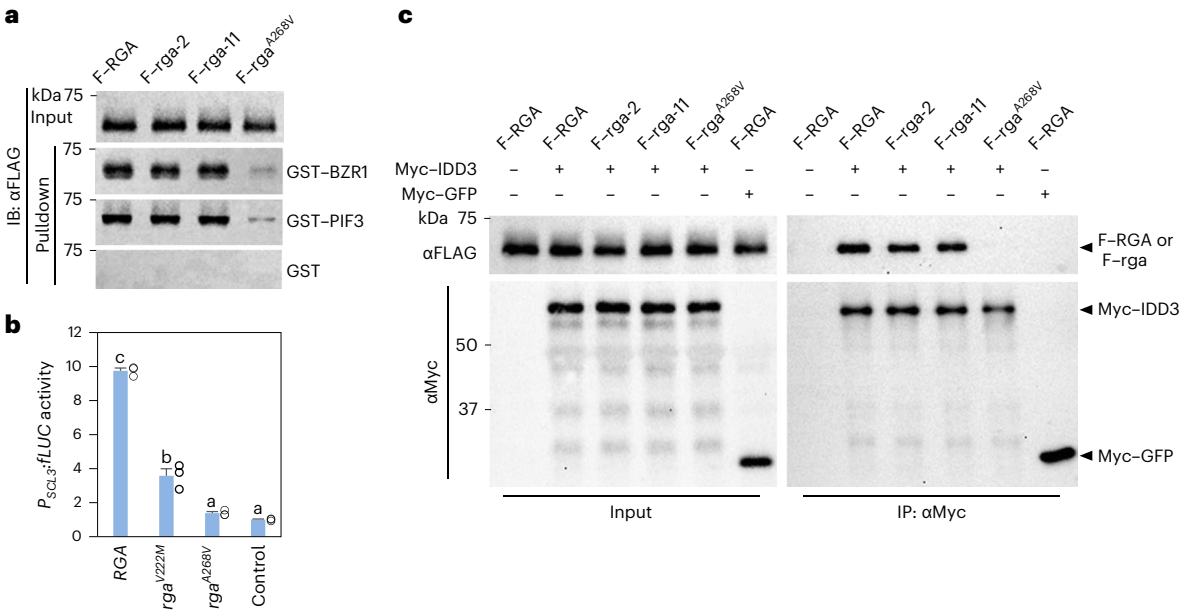

Fig. 4 | Pulldown and co-IP assays showed rga mutations in the LHR1 subdomain reduced interaction with BZR1, PIF3 and IDD3, whereas rga-2 and rga-11 in PFYRE did not. a, In vitro pulldown assay showing much reduced interaction of rga^{A268V} with BZR1 and PIF3. Recombinant GST, GST–BZR1 and GST–PIF3 bound to glutathione–Sepharose beads were used separately to pull down FLAG–RGA or FLAG–rga from protein extracts from transgenic *Arabidopsis* in the *ga1 dP* background. Immunoblots containing input *Arabidopsis* extracts and pulldown samples were detected with an anti-FLAG antibody. IB, immunoblot. Ponceau S-stained blots indicated that similar amounts of the GST or GST-fusion proteins were used in each set of the pulldown assays (Supplementary Fig. 4a). Representative images of three biological repeats are shown. **b**, *rga*^{V222M} and *rga*^{A268V} showed impaired activation of P_{SCL3}:*fLUC*. The dual LUC assay in the *N. benthamiana* transient expression system was performed as described in Fig. 2a. RGA and rga proteins were expressed at similar levels in these assays (Supplementary Fig. 2c). Means ± s.e. of three biological replicates are shown. The relative P_{SCL3}:*fLUC* activity in the control sample was set to one. Statistical analyses were performed with two-tailed Student's *t*-tests. Different letters above the bars represent significant differences, $P < 0.01$. Exact *P* values are listed in Source Data Fig. 4. **c**, Co-IP assay showing rga^{A268V} was not immunoprecipitated by Myc–IDD3. FLAG–RGA and FLAG–rga were expressed alone or co-expressed with Myc–IDD3 or Myc–GFP–NLS in *N. benthamiana* as indicated. An anti-Myc agarose was used for IP, and protein blots were probed with anti-Myc and anti-FLAG antibodies, separately. Representative images of two biological repeats are shown.

PIFs, IDD3 or TCP14, and indicate that PFYRE may have an unidentified role for RGA activity.

Previous studies suggest that the LHR1 subdomain of the DELLA proteins is required for binding many DELLA-interacting proteins (for example, BZR1, PIFs, TCPs and IDDs). However, this conclusion was based on Y2H and in vitro pulldown assays using serial truncations of DELLA proteins, which complicated the interpretation of results because deletions of the C-terminal GRAS subdomains often also abolish protein–protein interactions[8]. Thus, we further analysed the role of LHR1 using missense mutants. Among the *rga* mutants that we generated, the only *rga* mutation in the LHR1 subdomain, *rga-15*, displayed a relatively weak phenotype (Fig. 1d,e and Supplementary Fig. 3c). However, several missense *della* mutations in conserved residues within LHR1 (α1 and α3) that conferred strong phenotypes were identified in *DELLA* orthologs in barley (*SLENDER1* (*SLN1*)) and wheat (*REDUCED HEIGHT* (*RHT*))[40]. We created two new *rga* alleles within LHR1, *rga*^{V222M} and *rga*^{A268V}, corresponding to *rht-2* and *rht-7* in wheat, respectively, by site-directed mutagenesis to study the role of LHR1 further. We first tested the activity of these new rga mutant proteins by assaying P_{SCL3}:*fLUC* reporter expression in the transient expression system in *N. benthamiana*. The rga^{A268V} mutation (rht-7) completely abolished RGA-induced *SCL3* promoter expression, whereas the rga^{V222M} mutation (rht-2) showed an intermediate defect in this assay (Fig. 4b and Supplementary Fig. 2c). The rga^{A268V} mutant protein also failed to interact with BZR1, PIF3 and IDD3 by Y2H assays; showed much weaker binding to TCP14; and abolished the self-activation activity of RGA, possibly by altering RGA interaction with unidentified yeast protein(s) (Fig. 3a). These results support that *rga*^{A268V} is a strong allele. To verify the effect of *rga*^{A268V} in planta, we generated transgenic *Arabidopsis* lines that carry P_{RGA}:*FLAG–rga*^{A268V} in the *ga1 dP* background. Indeed, P_{RGA}:*FLAG–rga*^{A268V} did not show any growth suppression activity, whereas P_{RGA}:*FLAG–RGA* restored the dwarf phenotype in the *ga1 dP* background (Fig. 3b,c and Supplementary Fig. 3a,b). A pulldown assay further showed that FLAG–rga^{A268V} in the *Arabidopsis* extracts interacted very weakly with BZR1 and PIF3 compared with FLAG–RGA, rga-2 or rga-11 (Fig. 4a and Supplementary Fig. 4a), which is consistent with the Y2H results in Fig. 3a. A similar pulldown assay was not applicable using the recombinant IDD3 fusion protein. Therefore, we performed a co-IP assay to examine the effect of rga^{A268V} on IDD3 binding using *N. benthamiana* that co-expressed Myc–IDD3 and FLAG–RGA or FLAG–rga (Fig. 4c). Myc–GFP was included as a negative control. FLAG–rga-2 and FLAG–rga-11 were similarly co-immunoprecipitated with Myc–IDD3 compared with FLAG–RGA, whereas FLAG–rga^{A268V} was not detectable in the immunoprecipitated sample.

Taken together, the above results provided strong evidence that while both LHR1 and PFYRE subdomains are central for DELLA function, only LHR1 is required for binding to BZR1, PIF3, IDD3 and TCP14.

PFYRE subdomain is required for RGA binding to target chromatin

Although DELLA proteins do not contain canonical DNA-binding motifs, RGA was shown to associate with promoters of its target genes by ChIP–qPCR[19]. More recently, ChIP–seq analyses identified global RGA binding loci (2,327 genes) in the inflorescence meristem, using a gain-of-function *GFP–rgaΔ17* transgenic line[20] (rgaΔ17 contains an in-frame deletion of the DELLA motif for GA/GID1-induced degradation[12]), and in seedlings (~400 genes), using a *GFP–RGA* transgenic line[21]. Many of the RGA binding peaks are enriched near *cis*-elements for TFs.

https://doi.org/10.1038/s41477-023-01477-y

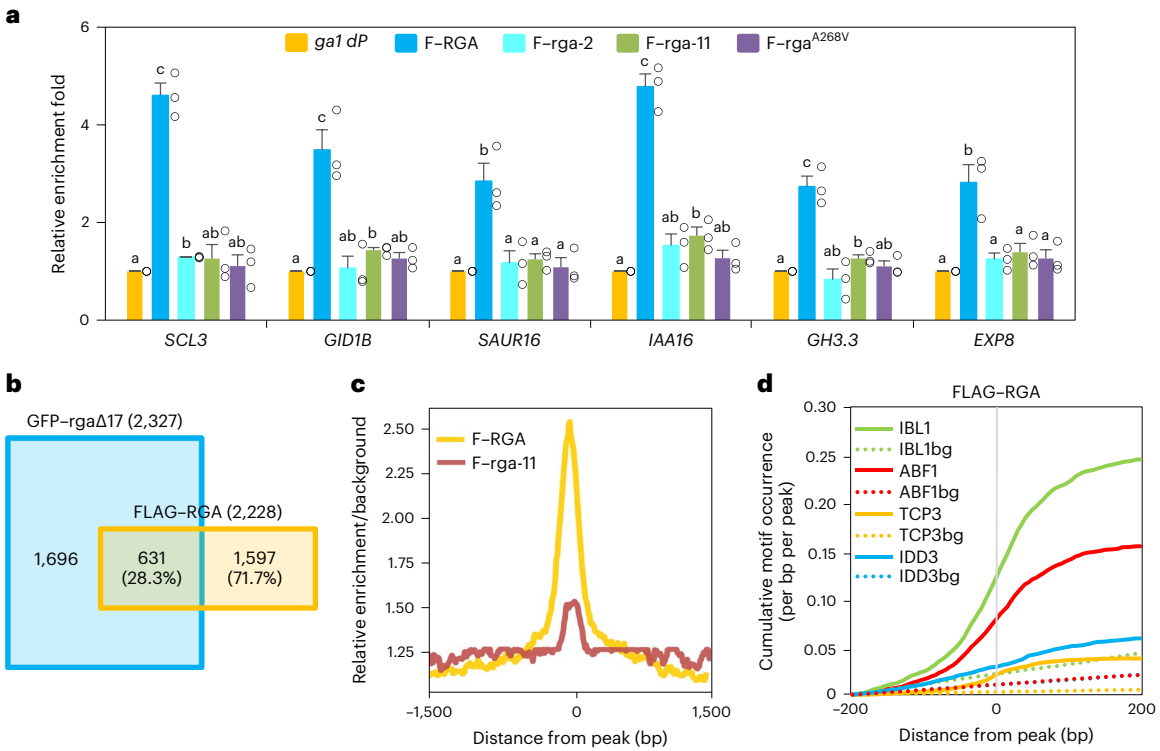

Fig. 5 | rga mutations in the PFYRE subdomain impaired association with target chromatin globally by ChIP–seq analysis. a, ChIP–qPCR analysis of six selected RGA direct target genes, showing *rga-2*, *rga-11* and *rga*^{A268V} abolished binding to target chromatin. ChIP was performed using transgenic lines containing P_{RGA}*:FLAG–RGA* or P_{RGA}*:FLAG–rga* in the *ga1 dP* background as labelled. The parental line *ga1 dP* was included as a control. Two RGA-activated genes (*SCL3* and *GID1B*) and four RGA-repressed genes (*SAUR16*, *IAA16*, *GH3.3* and *EXP8*) were tested by ChIP–qPCR using primers near the RGA binding peaks. The relative enrichment fold was calculated by normalizing against ChIP–qPCR of non-transgenic *ga1 dP* control using *PP2A*. Means ± s.e. of three biological replicates are shown. Different letters above the bars represent significant differences ($P < 0.05$) by two-tailed Student's *t*-test. Exact *P* values are listed in Source Data Fig. 5. **b**, A Venn diagram showing the overlap between genes adjacent to the binding sites of GFP-rgaΔ17 (ref. 20) and FLAG–RGA (this study). ChIP–seq was performed using transgenic lines containing P_{RGA}*:FLAG–RGA* or P_{RGA}*:FLAG–rga-11* in the *sly1 dP* background. The *sly1 dQ* (*RGA*) and *sly1 dP* lines were included as controls. All genes adjacent to a binding peak are listed in Supplementary Table 3. **c**, Genome-wide relative enrichment over background. The ratios of ChIP–seq read counts compared with the background were calculated for every 5 nt bins within 1.5 kb of the high-confidence FLAG–RGA peak positions using deepTools. We plotted the median values of the ratios of FLAG–RGA and FLAG–rga-11, compared with their respective background, for all peak positions. **d**, Cumulative motif occurrence in the genomic regions from −200 bp to +200 bp of the FLAG–RGA peak locations. All motifs significantly enriched within 200 bp of the peaks ($P < 0.01$, hypergeometric enrichment test, one-tailed; $q < 0.027$ after Benjamini–Hochberg correction) are listed in Supplementary Table 4. Among bHLH, bZIP, TCP and IDD TFs, IBL1, ABF1, TCP3 and IDD3, whose binding *cis*-elements were the most enriched, are shown as representative. Dotted lines indicate background (bg) level of motif occurrence at random genomic locations. Source data for **d** are provided in Source Data Fig. 5.

These previous findings support the current model that RGA and other DELLAs are recruited to target promoters via interacting TFs that bind specific *cis*-elements. As described above, the *rga-2* and *rga-11* mutations within the PFYRE subdomain abolished the growth suppression activity of RGA in planta, although they did not affect binding of the TFs BZR1, PIF3, IDD3 or TCP14. To decipher the molecular function of the PFYRE subdomain, we examined whether *rga-2* and *rga-11* affect RGA association with target chromatin in planta. ChIP–qPCR analysis was performed using transgenic *Arabidopsis* lines carrying P_{RGA}*:FLAG–RGA*, P_{RGA}*:FLAG–rga-2* or P_{RGA}*:FLAG–rga-11* in the *ga1 dP* background. Importantly, both FLAG–rga-2 and FLAG–rga-11 showed a notably reduced association with promoters of two known RGA-activated direct target genes, *SCL3* and *GID1B* (Fig. 5a). To determine whether the PFYRE subdomain is essential for RGA association with target chromatin globally, ChIP–seq was performed using transgenic *Arabidopsis* lines (in the *sly1 dP* background) carrying P_{RGA}*:FLAG–RGA* versus P_{RGA}*:FLAG–rga-11*, and two negative controls *sly1 dQ* (quadruple *della* with *RGA*) and *sly1 dP*. Candidate genes were defined as those containing at least one FLAG–RGA binding peak between −3 kb 5′-upstream and 1.5 kb 3′-downstream of the coding sequences, but not in the non-transgenic *sly1 dQ* controls. High-confidence peaks were selected by using the enrichment fold of a known RGA direct target gene *GID1B* as the cut-off (Supplementary Table 2), and a total of 2,228 genes near 1,558 FLAG–RGA binding peaks were identified ($q < 10^{-3}$). The *q* values were calculated by the Benjamini–Hochberg correction for multiple testing. (Supplementary Table 3). We performed ChIP–qPCR assays and the results further confirmed FLAG–RGA binding to four selected candidate genes, *SAUR16*, *IAA16*, *GH3.3* and *EXP8*, which are RGA-repressed genes (Fig. 5a). In addition, 631 genes near FLAG–RGA binding peaks (28.3%) were associated with GFP–rgaΔ17 binding peaks reported previously (2,327 genes near 1,677 peaks; with WT as their control; $q < 10^{-3}$)[20] (Fig. 5b and Supplementary Table 3). The 28.3% overlap is probably due to the differences in tissue types and RGA fusion proteins used for the two studies: young seedlings for FLAG–RGA ChIP–seq and inflorescence meristems for GFP–rgaΔ17 ChIP-seq. Nevertheless, among the 631 overlapping genes, the two ChIP–seq datasets showed remarkable consistency in RGA versus GFP–rgaΔ17 binding peak positions, with 86.1% of the relative peak summit positions within ±200 bp (Supplementary Table 3). Genome browser images around six RGA target genes showed overlapping FLAG–RGA and GFP–rgaΔ17 binding peaks near these genes (Supplementary Fig. 5a). By binding profile analysis, we found that the majority of FLAG–RGA binding peaks were in promoter regions

https://doi.org/10.1038/s41477-023-01477-y

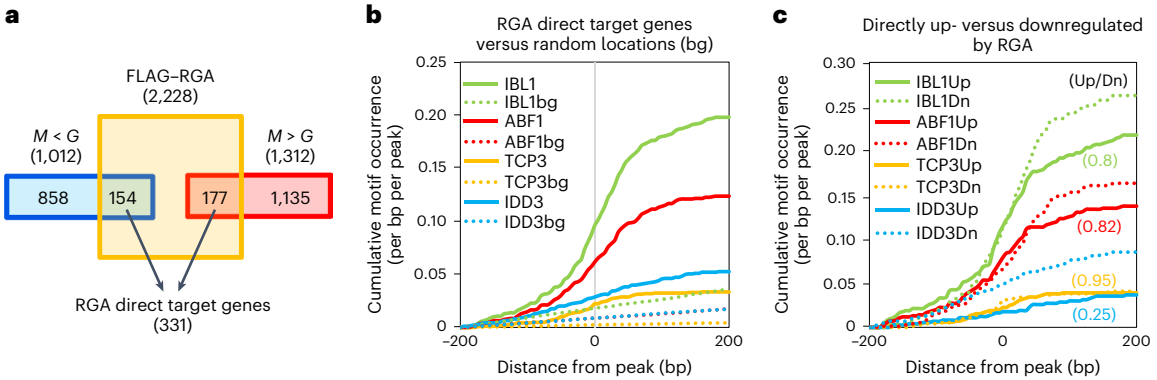

Fig. 6 | *cis*-Elements for bHLH, bZIP, TCP and IDD TFs were most enriched near RGA binding peaks associated with RGA direct target genes. a, Identification of RGA direct target genes. Genes located near a FLAG–RGA peak that are GA-responsive (based on an RNA-seq dataset[37]) were considered as RGA direct targets (Methods). RGA acts as 'direct repressor' and 'direct activator' on 154 and 177 genes, respectively. The list of all RGA direct target genes is in Supplementary Table 3. **b**, Cumulative occurrence of representative motifs enriched near FLAG–RGA peaks close to RGA direct target genes. Binding motifs for representative TFs, IBL1 (bHLH), ABF1 (bZIP), TCP3 (TCP) and IDD3 (IDD), are shown as in Fig. 5d. **c**, Comparison of motif occurrence between FLAG–RGA peaks close to 177 RGA direct activated genes (Up) and 154 RGA direct repressed genes (Dn) identified in **a**. Ratios in parentheses indicate the fold difference between peaks near RGA direct activated genes and repressed genes, after subtracting background (that is, random locations) cumulative occurrences. Source data for **b** and **c** are provided in Source Data Fig. 6. G, GA treatment; M, mock treatment; M < G, GA-upregulated genes; M > G, GA-downregulated genes.

(Supplementary Fig. 5b), which is consistent with the function of RGA. ChIP–seq using FLAG–rga-11 identified 196 binding peaks (associated with 313 genes) with only 79 genes that are near RGA binding sites. Strikingly, most of the RGA binding peaks (96.5%) were not detected by the mutant protein FLAG–rga-11 (Supplementary Table 3 and Supplementary Fig. 6a). Compared with the binding of RGA, the genome-wide enrichment over binding peak regions was substantially reduced by the *rga-11* mutation (Fig. 5c). Genome browser images around six selected RGA target genes showed that *rga-11* abolished its binding to these loci (Supplementary Fig. 6b). ChIP–qPCR analysis further showed that, like *FLAG–rga-11*, *FLAG–rga-2* also abolished binding to all six selected target genes (Fig. 5a).

cis-Elements for many TFs were enriched near RGA binding peaks

All *cis*-elements that were significantly enriched near binding peaks of FLAG–RGA and GFP–rgaΔ17 are listed in Supplementary Table 4. Among them, we found most significant enrichments for *cis*-elements of members from four TF families (bHLH, bZIP, TCP, and IDD) near both FLAG–RGA binding peaks (Fig. 5d, Supplementary Fig. 5c and Supplementary Table 4) and GFP–rgaΔ17 binding peaks (Supplementary Table 4). *cis*-Elements of additional TF families were identified, including C2C2-Dofs, Homeobox, CAMTAs, AP2-EREBPs, WRKYs, MYBs, NACs, SPLs, MADS, ARF and GRF. All these TF families, except CAMTAs, were reported to be potential DELLA interactors, although some were previously identified only through Y2H assays[23].

Because RGA is rapidly degraded upon GA treatment[11], we considered genes showing both differential expression by GA treatment and FLAG–RGA binding as direct targets of RGA. Therefore, we looked for overlapping genes between the genes near the FLAG–RGA binding peaks in this study with GA-responsive genes in a previously published RNA-sequencing (RNA-seq) dataset[37]. We identified 177 and 154 genes where RGA may act as a direct activator (downregulated by GA; that is, higher expression with the presence of DELLA) or a repressor (upregulated by GA), respectively (Fig. 6a and Supplementary Table 3). Almost all of these 331 RGA direct target genes, except 13, were undetectable by ChIP–seq using FLAG–rga-11 (Supplementary Fig. 6c and Supplementary Table 3). Gene Ontology terms enriched in direct RGA targets are shown in Supplementary Table 5. RGA-activated target genes include positive regulators of GA signalling (for example, GA receptors *GID1A* and *GID1B*), GA-repressed genes (*SCL3*, *GASA1*, *GA2OOX2*, *BOI* and *IDD22*), ABA signalling components (for example, *ABI5, PP2C, RHA2B and AtHB6*), genes that are responsive to biotic or abiotic stresses (cold and water stresses), and regulation of transcription and RNA metabolism. RGA-repressed target genes are in general involved in growth processes, including auxin metabolism and signalling (for example, *SAURs*, *IAAs* and *GH3.6*), cell wall organization/biogenesis and cell growth (for example, *EXPs*, *PMEs* and *FLAs*), cell division and cell differentiation.

FLAG–RGA binding peaks located near the 331 direct target genes of RGA showed enrichment of *cis*-elements for multiple TFs in bHLH, bZIP, TCP and IDD families (Supplementary Table 4), represented in Fig. 6b by IBL1, ABF1, TCP3 and IDD3, respectively. Interestingly, although IBL1, ABF1 and TCP3 showed similar motif occurrence patterns between RGA-activated and -repressed genes, binding motifs for IDD3 were enriched in the FLAG–RGA peaks adjacent to RGA-activated genes (Fig. 6c), which is consistent with a previous report showing DELLA acting as a co-activator of IDD3[33]. Several members of these four TF families have been shown to interact with DELLAs[22–25,31–34], supporting the idea that RGA is recruited to target chromatin by binding to these TFs.

RGA binding to target genes also requires its LHR1 subdomain

Previous studies reported two distinct modes of DELLA action: (1) DELLA-mediated transcription activation of target genes (for example, *SCL3*) requires its recruiting TFs (for example, IDDs), which bind to both DELLA and the target promoter sequences; and (2) DELLA alters transcription by sequestration of transcription activators (for example, BZR1, PIFs and TCPs) or repressors (for example, JAZs) from target promoters[7,8]. Based on this model, DELLA proteins should only be associated with chromatin of DELLA-activated genes (first mode of action), but not with DELLA-repressed or -activated genes via the second mode of action. However, our ChIP–seq and ChIP–qPCR results showed that RGA binding peaks are near both RGA-activated and -repressed genes (Figs. 5a and 6a). Similarly, GFP–rgaΔ17 binding peaks reported previously[20] are also near RGA-activated and -repressed genes (Supplementary Fig. 5d). Based on these observations, we proposed an alternative model in which RGA is recruited to all its target chromatin by binding to specific TFs, regardless of its additive or antagonistic role in transcriptional activation or repression. According to our model, the rga^{A268V} (LHR1 subdomain mutation) that is impaired in binding TFs should also have a defect in chromatin binding globally.

https://doi.org/10.1038/s41477-023-01477-y

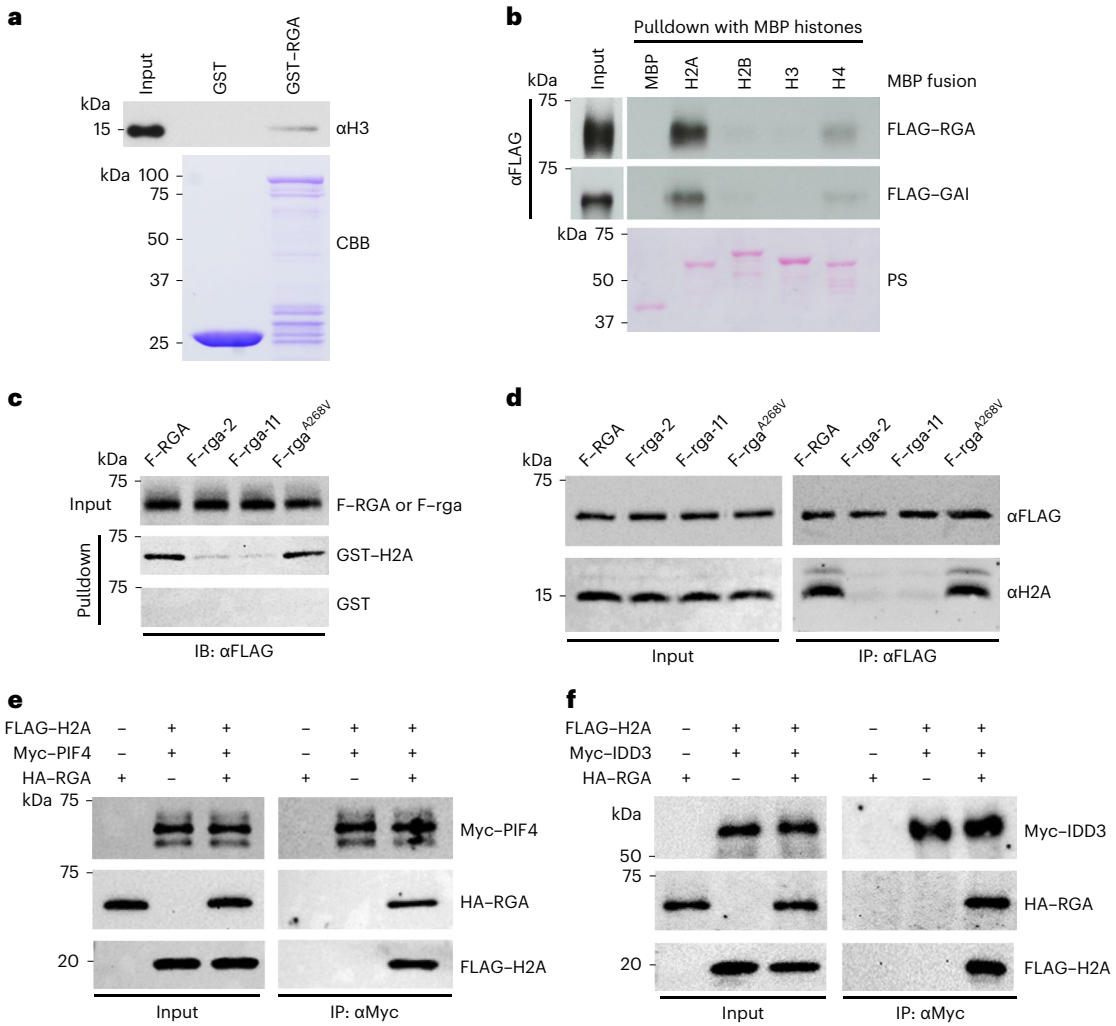

Fig. 7 | *rga-2* and *rga-11* reduced RGA binding to histone H2A. a, GST–RGA pulled down calf thymus histones. GST and GST–RGA bound to glutathione beads were mixed separately with calf thymus nucleosomes. Immunoblot containing the input (0.01 μg calf thymus histones) and pulldown samples were probed with an anti-H3 antibody. Coomassie Brilliant Blue (CBB)-stained gel shows the amounts of GST and GST–RGA used in the pulldown assay. **b**, MBP–H2A pulled down FLAG–RGA and FLAG–GAI from extracts of *N. benthamiana* expressing FLAG–RGA and FLAG–GAI. Recombinant MBP and MBP–H2A, MBP–H2B, MBP–H3 and MBP–H4 bound to amylose resin were used separately in the pulldown assay. Ponceau S staining showed MBP and MBP fusion proteins. **c**, GST–H2A pulled down FLAG–RGA more efficiently than FLAG–rga-2 and FLAG–rga-11 proteins from *Arabidopsis* extracts, but rga^{A268V} mutation did not affect H2A binding. GST and GST–H2A bound to glutathione beads were used separately to pull down FLAG–RGA or FLAG–rga from protein extracts of transgenic *Arabidopsis* (in *ga1 dP* background) carrying P_{RGA}*:FLAG–RGA/rga* as labelled. Immunoblots containing input *Arabidopsis* extracts and pulldown samples were detected with an anti-FLAG antibody. Ponceau S-stained blots indicated that similar amounts of the GST or GST–H2A proteins were used in each set of the pulldown assays (Supplementary Fig. 4a). **d**, Co-IP assay showing the endogenous H2A was co-immunoprecipitated by FLAG–RGA and FLAG–rga^{A268V}, but not by FLAG–rga-2 or FLAG–rga-11. FLAG–RGA and FLAG–rga from protein extracts of transgenic *Arabidopsis* (in *ga1 dP* background) carrying P_{RGA}*:FLAG–RGA/rga* were immunoprecipitated using an anti-FLAG antibody. Immunoblots containing input *Arabidopsis* extracts and immunoprecipitated samples were detected with anti-FLAG and anti-H2A antibodies, separately. **e**, Detection of PIF4–RGA–H2A complex by co-IP. Myc–PIF4, HA–RGA and FLAG–H2A were transiently expressed alone or co-expressed in *N. benthamiana* as indicated. **f**, Detection of the IDD3–RGA–H2A complex by co-IP. Myc–IDD3, HA–RGA and FLAG–H2A were transiently expressed alone or co-expressed in *N. benthamiana* as indicated. In **e** and **f**, Myc–PIF4 and Myc–IDD3 were immunoprecipitated from protein extracts using anti-Myc agarose. Protein blots were probed with anti-Myc, anti-HA and anti-FLAG antibodies separately. Representative images of two (**a**, **b** and **f**) or three (**c**–**e**) biological repeats are shown, and source data are provided in Source Data Fig. 7.

Indeed, ChIP–qPCR analysis showed that FLAG–rga^{A268V} failed to bind six selected target promoters, including two RGA-activated and four RGA-repressed genes (Fig. 5a). Our model also predicts RGA and its antagonizing TFs co-localize to target chromatin. We searched for PIF4-induced genes that are associated with both RGA and PIF4 binding peaks using published PIF4 ChIP–seq and RNA-seq datasets[53], and found a total of 150 overlapping genes (Supplementary Table 6 and Supplementary Fig. 7a). Among them, we observed a high degree of co-occurrence of RGA and PIF4 binding peaks, with 70.7% (106 genes) of the peak summit positions being within ±100 bp (Supplementary Table 6). Genome browser images around six selected PIF4-induced target genes showed overlapping RGA and PIF4 binding peaks (Supplementary Fig. 7b).

Taken together, mutations in either the LHR1 (rga^{A268V}) or PFYRE subdomain (rga-2 and rga-11) of RGA led to a much reduced association with target chromatin. However, only rga^{A268V} was dramatically impaired in binding of TFs BZR1, PIF3, IDD3 or TCP14, whereas the PFYRE subdomain mutations did not notably affect binding to these TFs. These findings suggest that additional factor(s) are required to stabilize RGA's association with target chromatin, presumably after

https://doi.org/10.1038/s41477-023-01477-y

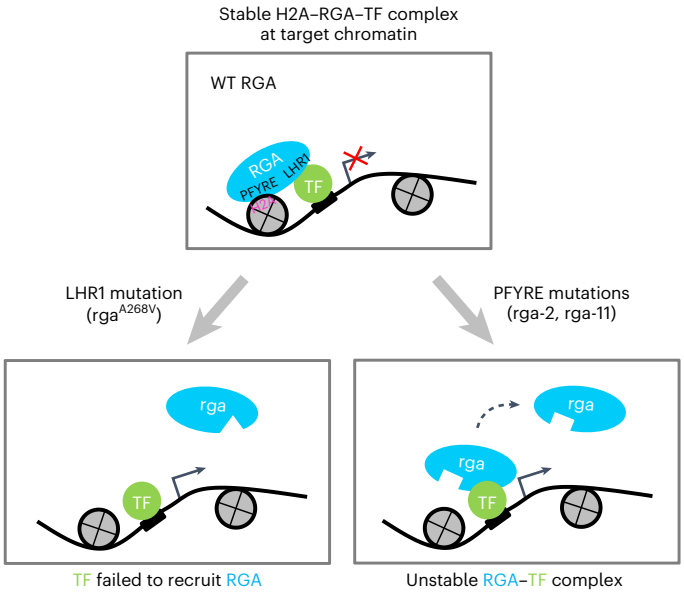

Fig. 8 | Working model of DELLA-mediated transcriptional regulation. DELLA proteins (for example, RGA) are recruited to target chromatin by interaction with TFs via the LHR1 subdomain. The transient TF–RGA interaction is stabilized by RGA–H2A binding (via its PFYRE subdomain) to form TF–RGA–H2A complexes at the target chromatin. Mutations in the LHR1 subdomain (for example, rga^{A268V}) prevent recruitment to target chromatin by the TFs. In contrast, mutations in the PFYRE subdomain (for example, rga-2 and rga-11) abolish H2A binding. Both subdomains are essential for DELLA-mediated transcription repression and activation. The diagram only depicts RGA-mediated transcription repression. A similar diagram can depict RGA-mediated transcription activation, except that the TF–RGA–H2A complex will promote transcription of target genes and that either LHR1 or PFYRE mutations will reduce transcription.

RGA binding to TFs, and α10 within the PFYRE subdomain plays a key role in this interaction.

RGA binding to histone H2A via its PFYRE subdomain

Our study on rga-2 and rga-11 (mutations in α10 within PFYRE subdomain) suggested that, besides interacting TFs, RGA association with target chromatin requires additional factors. To test whether RGA directly interacts with histones, in vitro pulldown assays were performed. We found that recombinant GST–RGA was able to pulldown calf thymus histones (histone complexes containing H1 and H2A/H2B/H3/H4 core) (Fig. 7a). We then compared the binding affinity between RGA and individual histone proteins by a pulldown assay using FLAG–RGA that was transiently expressed in *N. benthamiana*, and individual histone proteins expressed in *E. coli* as MBP fusion proteins. We found that FLAG–RGA was pulled down strongly by MBP–H2A and weakly by MBP–H4, but not by MBP or other histone fusions (Fig. 7b). In addition to RGA, H2A also pulled down another *Arabidopsis* DELLA protein, GAI (Fig. 7b). To test whether mutations in the LHR1 (rga^{A268V}) and PFYRE (rga-2 and rga-11) subdomains affect H2A binding, an in vitro pulldown assay was performed using GST, GST–H2A, and protein extracts from *Arabidopsis* expressing FLAG–RGA or FLAG–rga proteins. Importantly, FLAG–rga-2 and FLAG–rga-11, but not FLAG–rga^{A268V}, showed reduced binding to H2A compared with FLAG–RGA (Fig. 7c and Supplementary Fig. 8a). To confirm RGA–H2A interaction in *Arabidopsis*, co-IP assays were performed. FLAG–RGA in protein extracts from the P_{RGA}*:FLAG–RGA/rga* transgenic plants were immunoprecipitated using anti-FLAG antibody, and then analysed by immunoblotting using anti-H2A and anti-FLAG antibodies, separately (Fig. 7d). H2A was co-immunoprecipitated with FLAG–RGA, supporting that H2A and RGA interact in planta. But H2A was not detected in FLAG–rga-2 or FLAG–rga-11 co-IP products, which is consistent with the in vitro pulldown results. In contrast, the interaction between FLAG–rga^{A268V} and H2A was similar to that of FLAG–RGA (Fig. 7d) These results indicate rga-2 and rga-11 (PFYRE mutations) abolish the interaction between RGA and H2A, which is distinct from the defect of rga^{A268V} (LHR1 mutation) in binding TFs. Our findings suggest that, once TFs recruit RGA via its LHR1 subdomain to target gene promoters, RGA–H2A interaction via its PFYRE subdomain is required to stabilize the H2A–RGA–TF complex at the target chromatin. To verify whether RGA binds to both H2A and its interacting TF in a complex, we performed co-IP assays by expressing epitope-tagged RGA, PIF4 and/or H2A in *N. benthamiana*. Myc–PIF4 was able to pulldown both HA–RGA and FLAG–H2A, whereas Myc–PIF4 did not pulldown FLAG–H2A in the absence of RGA (Fig. 7e). These results support the formation of the PIF4–RGA–H2A complex in planta. Co-IP assays were also performed using epitope-tagged RGA, IDD3 and/or H2A, and similar results were observed that support IDD3–RGA–H2A complex formation in planta (Fig. 7f).

H2A monoubiquitination (H2Aub1) and replacement of H2A with the H2A variant H2A.Z have been reported to regulate gene transcription in eukaryotes, including plants[54–56]. In *Arabidopsis*, H2Aub1 is enriched in many transcriptionally repressed genes. However, recently it has also been found to be located in transcriptional regulation hot spots, which have less accessibility, but are still permissive chromatin[57,58]. H2A.Z is enriched at +1 nucleosome (the first nucleosome downstream of the transcription start site (TSS)) in actively transcribed genes, but it can play a repressive role when located in gene bodies[59,60]. Monoubiquitination of H2A.Z appears to correlate with its repressive role in transcription[61]. A co-IP assay using transient expression in *N. benthamilana* showed that RGA binds to H2A and H2A.Z similarly (Supplementary Fig. 8b). To further investigate the relationship between RGA and H2Aub1 or H2A.Z, we compared genome-wide RGA binding peak positions to H2Aub1 and H2A.Z distribution using published ChIP–seq datasets[58,62] (Supplementary Fig. 9a,d and Supplementary Table 7). Neither H2Aub1 nor H2A.Z peak locations co-localized with the RGA binding peak (Supplementary Fig. 9b,d). The average RGA binding peak is located at approximately 200 nucleotides (nt) 5′-upstream of the TSS, and then sharply decreased around the TSS (Supplementary Fig. 9e), indicating that RGA does not interact with the +1 nucleosome, the positioning of which is based on nucleosome profiling in WT seedlings detected by micrococcal nuclease sequencing[63].

To investigate whether RGA binding affects target chromatin accessibility, we performed assay for transposase-accessible chromatin sequencing (ATAC-seq) using P_{RGA}*:FLAG–RGA* and P_{RGA}*:FLAG–rga-11* transgenic lines in the *sly1 dP* background. Principle component analysis showed that two biological replicates of each genotype clustered together (Supplementary Fig. 10a). Analysis of our ATAC-seq dataset identified 379 differentially accessible regions (DARs) near 689 genes (false discovery rate ≤ 0.05) between *FLAG–RGA* and *FLAG–rga-11* lines (Supplementary Table 8). Among them, 82 genes contain FLAG–RGA binding peaks, 108 genes are GA-responsive and only 20 are RGA direct target genes (that is, genes that are associated with RGA binding peaks and are GA-responsive) (Supplementary Fig. 10b). If RGA binding caused altered target chromatin accessibility, GA-repressed (RGA-induced) genes should display reduced accessibility in *FLAG–rga-11* than in the *FLAG–RGA* line, whereas GA-induced (RGA-repressed) genes should show increased accessibility. However, scatterplot analysis of the 108 GA-responsive genes with DARs (*FLAG–rga-11* versus *FLAG–RGA* line) did not show any correlation between chromatin accessibility and GA responsiveness (Supplementary Fig. 10c). In addition, most of the RGA direct target genes (n = 311, 94%) did not show differential accessibility between *RGA* and the *rga-11* mutant. The overall RGA binding peak regions for these 311 target genes co-localized with an accessible peak (ATAC-seq) near the TSS, although *rga-11* did not alter chromatin accessibility (Supplementary Fig. 10d). Genome browser images around six selected RGA target genes further showed

that chromatin accessible peak(s) near individual gene in both *RGA* and *rga-11* backgrounds co-localized with RGA binding peak(s) (Supplementary Fig. 10e). These results indicate that RGA appears to bind to accessible chromatin, whereas RGA binding does not significantly alter target chromatin structure as detected by ATAC-seq.

Discussion

Our study shows that the DELLA–H2A interaction is essential for DELLA-mediated global transcription reprogramming, and that DELLA proteins require at least two functionally distinct subdomains (LHR1 and PFYRE) within their C-terminal GRAS domain for transcription regulation (Fig. 8). These two subdomains form the α-helical cap of the GRAS domain (Fig. 1b), and they appear to play distinct roles in interacting with different groups of regulatory proteins. The LHR1 subdomain (α1–α3) is necessary for interactions with TFs, whereas the PFYRE subdomain (α10–α11) is essential for H2A binding. Mutations in either subdomain abolished RGA association with target chromatin globally (Fig. 8). We also confirmed the formation of PIF4–RGA–H2A and IDD3–RGA–H2A protein complexes in planta by co-IP assays. Based on these results, we propose that RGA (and other DELLAs) are recruited to target promoters via TFs that recognize specific *cis*-elements, and the transient TF–RGA interaction (via the LHR1 subdomain) is stabilized by RGA–H2A binding (via its PFYRE subdomain) to form TF–RGA–H2A complexes at the target chromatin. Our meta-analysis indicated that the genome-wide RGA binding peak position does not co-localize with H2Aub1, H2A.Z or the +1 nucleosome. Considering the average RGA binding peak is located at approximately 200 nt 5′-upstream of the TSS, it is possible that RGA (and other DELLAs) interact with H2A of nearby nucleosomes in the promoter region after being recruited to target chromatin by specific TFs.

We also found that RGA binding peaks are located near both RGA-activated and RGA-repressed genes by combining the RGA ChIP–seq results (this study) and an RNA-seq dataset (for GA-responsive genes)[37]. The association of RGA at RGA-repressed promoters was unexpected based on the current model for direct sequestration of transcription activators (for example, BZR1, PIFs and TCPs) by RGA. Considering the findings in this study, it is likely that RGA (and other DELLA proteins) are initially recruited to all its target chromatin by binding to specific TFs and forming TF–DELLA–H2A complexes to repress or activate transcription of target genes. For DELLA-mediated transcription repression, DELLA either directly interferes with TF transactivation or recruits co-repressor(s) once the TF–RGA–H2A complex is formed. It remains possible that DELLA binding may result in subsequent reduction in TF binding to target DNA. For DELLA-mediated transcription activation, DELLA may function as a co-activator as it displays transactivation activity in yeast and in plant cells[41,48]. DELLA may also recruit other co-activator(s) after forming the TF–RGA–H2A complex at the target chromatin. Thus, DELLA-mediated transcription activation versus repression at an individual promoter is probably dependent on interacting TFs and co-activators or co-repressors. In addition, DELLA interacts with chromatin remodellers (SWI/SNF, and PKL)[35–37]. Genetic analysis indicates that most GA-mediated developmental processes require the CHD3 chromatin remodeller PKL[37], which antagonistically interacts with DELLA to promote GA responses[36]. Intriguingly, RNA-seq data showed that PKL function is required for GA induction of 310 vegetative growth-related genes (in the C2 cluster, including many DELLA-repressed genes, such as *EXP8*, *IAA19*, *SAURs* and *GH3.3*)[37]. In contrast, 468 GA-repressed genes (in the C5 cluster, including many DELLA-induced genes, such as *SCL3*, *GID1A*, *GID1B* and *GA2ox2*) are PKL independent. However, GA repression of another 356 genes (in C6 and C8 gene clusters) depends on PKL function[37]. Therefore, the precise role of PKL in regulating GA- and DELLA-responsive genes requires further investigation.

Our ATAC-seq analysis using *FLAG–RGA* and *FLAG–rga-11* lines (in a *sly1 dP* background) showed that most RGA binding sites correspond to accessible regions of target chromatin whose accessibility did not change in the presence or absence of functional RGA, suggesting that RGA is not responsible for the initial opening of target chromatin. This finding is consistent with recent studies showing that recruitment of DELLA and SPL9 to the *AP1* promoter for promoting flower initiation requires LEAFY[64], which functions as a pioneer TF for binding to target DNA in the nucleosome-occupied region and recruiting SWI/SNF chromatin remodellers to open chromatin[65].

In summary, our study provides insights into the complex mechanism of DELLA-mediated transcription reprogramming. We have identified a role of the PFYRE subdomain for binding H2A, which, together with the LHR1 subdomain, plays two distinct modular functions in DELLA-mediated genome-wide transcription regulation in plants.

Methods

Plant materials, growth conditions, plant transformation, GA treatment and statistical analyses

Plants were grown in the growth room or on plates as described previously[37]. For dim light treatment (Fig. 3b,c), seedlings were grown in 16 μmol m^{-2} s^{-1} light intensity under short-day (8 h light) conditions. The *ga1-3 rga* double mutants were screened and backcrossed to *ga1-3* once before characterization as described previously[4,46]. The *rga* mutants, *rga28* and *rga29*, containing transfer DNA insertion were reported in previous studies[66,67]. *sly1-10* (in the L*er* background)[68] was introgressed into the Col-0 background by backcrossing with Col-0 six times; *sly1-10 dellaP* (*sly1 dP*) and *sly1-10 dellaQ* (with WT *RGA*, *sly1 dQ*) were generated by crossing *sly1-10* (backcrossed to Col-0 six times) with *dellaP* (*rga-29*, SALK_089146; *gai-t6*, backcrossed to Col-0 six times; *rgl1*, SALK_136162; *rgl2*, SALK_027654; *rgl3-3*, CS16355)[67] and screening in F_2 and F_3 through phenotyping growth suppression and genotyping the transfer DNA insertion of the respective mutations. pRGA–His–3×FLAG–RGA, pRGA–His–3×FLAG–rga-2, pRGA–His–3×FLAG–rga-11 and pRGA–His–3×FLAG–rga-rht7 constructs (pCB–His–3×FLAG–RGA/rga, rht7 = rga^{A268V}) were transformed into *ga1-3 dellaP* (*ga1 dP*)[37] by floral dipping. *FLAG–RGA/rga sly1 dP* were obtained by crossing *sly1-10 dP* with *FLAG–RGA/rga ga1 dP* and screening the progenies in F_2 and F_3. The rga–CT2 transgenic line (L78-6923) in the L*er* background was described previously[45]. For early GA-response tests, plates with 8-day-growth plants were drenched with 10 μM GA_3 solution for 3 seconds and incubated in normal growth condition for the indicated time. Student's *t*-tests were performed for statistical analyses.

Plasmid construction

The following plasmids were described previously: P_{SCL3}:*fLUC* (ref. 48), pEG100–3F–GAI (35S:His–3×FLAG–GAI)[69], pCB–3F–RGA (pCB–His–3×FLAG–RGA), pEG100–3F–RGA (35S:His–3×FLAG–RGA), pCR8–GFPNLS, pEG3F–GW destination vector (containing His–3×FLAG-tag)[70] and pDONR207–3FR[45]. Primers and plasmid constructs are listed in Supplementary Tables 9 and 10, respectively. All DNA constructs generated from PCR amplification were sequenced to ensure that no mutations were introduced.

In silico prediction of 3D protein structure of the RGA GRAS domain

The 3D structure model of the RGA GRAS domain was built based on the structure of SCARECROW protein (5B3G)[49] as a template using the online SWISS-MODEL workspace (http://swissmodel.expasy.org/)[50,71]. Pymol package v.2.2.2 (https://pymol.org/) was run on the Python platform to visualize and locate the mutant alleles in the RGA GRAS model.

RT-qPCR analyses, immunoblot analyses and Y2H

Total RNA was isolated using the Quick-RNA MiniPrep kit (Zymo Research). Briefly, *Arabidopsis* seedlings (~60 mg) were ground in extraction buffer and processed following the manufacturer's

protocol. Reverse transcription was performed using M-MLV RTase (Promega) using anchored oligo(dT). For qPCR, the FastStart Essential DNA Green Master Mix was used with a LightCycler 96 (Roche Applied Science). Relative transcript levels were determined by normalizing with *PP2A* (At1g13320). Immunoblot analyses were performed using rabbit anti-RGA antiserum (DU176, 1:10,000 dilution)[11], horseradish peroxidase (HRP)-conjugated anti-FLAG M2 mouse monoclonal (A8592, 1:10,000 dilution; Sigma-Aldrich) and mouse HRP–anti-MYC monoclonal antibodies (catalogue number 626803, 1:1,000 dilution; BioLegend), mouse anti-HA monoclonal antibody (901503, 1:1,000 dilution; BioLegend), rabbit anti-H2A monoclonal antibody (catalogue number ab177308, 1:1,000 dilution; Abcam) and rabbit anti-histone 3 polyclonal antibody (catalogue number ab1791; Abcam). HRP-conjugated donkey anti-mouse IgG (catalogue number 715-035-150; Jackson ImmunoResearch) was used for anti-HA at a 1:10,000 dilution. HRP-conjugated goat anti-rabbit IgG (catalogue number 31462; Thermo Fisher) was used to detect anti-RGA and anti-HA at a 1:10,000 dilution. Y2H assays were performed as described previously[45].

Transient expression and dual LUC assay in *N. benthamiana*

For dual LUC assays and pulldown assays, transient expression of FLAG–RGA, FLAG–GAI and FLAG–rga in *N. benthamiana* was performed as described with slight modifications[48]. The *N. benthamiana* leaves were collected after 48 h of agro-infiltration[72]. Three biological repeats were conducted for each effector combination.

In vitro pulldown assay

In vitro pulldown assays using recombinant GST protein fusions expressed in *E. coli* BL21-CodonPlus (DE3)-RIL (Agilent Technologies) were performed following the procedures published previously with minor modifications[45]. To obtain the *N. benthamiana* lysate used for *in vitro* pulldown assays, leaves were infiltrated with *Agrobacterium* harbouring the corresponding binary vectors, collected after 2 days, ground in liquid nitrogen, and stored at −80 °C. Ground powder (100 mg) was resuspended in the *N. benthamiana* lysis buffer (50 mM Tris–HCl pH 8.0, 150 mM NaCl, 1% Triton X-100, 2.5 mM 2-mercaptoethanol and 1× protease inhibitor cocktail (Sigma-Aldrich)) and the slurry was passed through a 70 µm strainer by quick spinning. Flow through was collected and centrifuged at 4 °C, 15,000 rpm for 5 min. Lysate was obtained after spinning the supernatant again and used for the protein binding assays. The pulldown assays between FLAG–RGA or FLAG–GAI (from *N. benthamiana* protein extracts) and MBP–H2A, MBP–H2B, MBP–H3 and MBP–H4 (from *E. coli*) were performed using the same procedures, except that amylose resin (E8021S, lot number 0131305; New England BioLabs) was used to purify the MBP and MBP protein fusions, and plant lysis buffer of 200 mM NaCl was used for incubation and washing. The same procedure was used for pulldown assays between FLAG–PIF4 and FLAG–IDD3 (from *N. benthamiana* protein extracts) and MBP–RGA, MBP–rga-2 and MBP–rga-11 (from *E. coli*).

The pulldown assays using protein extracts from transgenic *Arabidopsis* lines (*FLAG–RGA ga1 dP, FLAG–rga-2 ga1 dP*, *FLAG–rga-11 ga1 dP* and *FLAG–rga-rht7 ga1 dP*) and recombinant proteins (GST, GST–BZR1, GST–PIF3 and GST–H2A) were performed in the same way as in FLAG–DELLA and MBP-histone binding assays, except that the ground *Arabidopsis* tissue powder was resuspended in the lysis buffer (50 mM Tris–HCl pH 8.0, 150 mM NaCl, 1% Triton X-100, 5 mM EDTA, 1× protease inhibitor cocktail (Sigma-Aldrich) and 1 mM PMSF).

For the calf thymus histone binding assay, glutathione bead charged with the GST–RGA was mixed with calf thymus histones (H9250; Sigma) in TBS buffer of 250 mM NaCl. After incubation at 4 °C with rotation for 2 h, the bead was washed five times with the same buffer. Interaction of RGA with histones was confirmed by immunoblot detection using anti-histone 3 antibody.

Co-IP

Total *Arabidopsis* protein was extracted from 0.5 g of ground powder in 2 ml of extraction buffer (50 mM Tris–HCl pH 8.0, 150 mM NaCl, 1% Triton X-100, 5 mM EDTA, 1× protease inhibitor cocktail (Sigma-Aldrich) and 1 mM PMSF) and centrifuged at 4 °C at maximum speed for 10 min. A 50 µl input was taken from the supernatant, and 1 ml protein extract was incubated with 20 µl anti-FLAG–M2–agarose beads (A2220; Sigma-Aldrich) for 1.5 h at 4 °C and then washed three times with wash buffer (50 mM Tris–HCl pH 7.5, 150 mM NaCl, 0.1% Tween-20). Samples were analysed by SDS–PAGE and immunoblotting using HRP-conjugated anti-FLAG antibody (Sigma-Aldrich) and anti-H2A antibody (Abcam) as described above.

To detect the PIF4–RGA–H2A or IDD3–RGA–H2A complex, MYC–PIF4 or MYC–IDD3, HA–RGA and FLAG–H2A were transiently expressed in *N. benthamiana* leaves and subsequent co-IP assays were performed using rabbit anti-Myc polyclonal antibody-conjugated agarose beads (A7470; Sigma-Aldrich), as described previously[45].

ChIP, ChIP–qPCR and construction of the ChIP library

For ChIP–qPCR analysis, transgenic *Arabidopsis* seedlings carrying P_{RGA}*:FLAG–RGA/rga* (in the *ga1 dP* background or the *sly1 dP* background) and the respective parental lines (*ga1 dP* or *sly1 dP*) were grown in continuous light for 10 days, harvested and cross-linked in 1% formaldehyde solution for 20 min. Seedlings were washed with water three times, snap-frozen and ground in liquid nitrogen. Around 100–200 mg of ground tissue powder was dissolved in 2 ml of nuclear isolation buffer (NIB) (0.25 M sucrose, 12 mM Tris–HCl pH 8.0, 5 mM $MgCl_2$, 60 mM KCl, 15 mM NaCl, 1 mM $CaCl_2$, 0.9% Triton X-100 and 1× protease inhibitor cocktail) and passed through the 70 µm strainer by quick spinning. Flow through was collected and spun at 3,000*g* for 5 min. After removing the supernatant, the pellet was resuspended in 1 ml NIB by pipetting and spun at 3,000*g* for 5 min. Rinsed pellet was resuspended in 500 µl of nuclear lysis buffer (50 mM Tris–HCl pH 8.0, 150 mM NaCl, 1 mM EDTA, 0.1% SDS, 0.1% Na deoxycholate, 1% Triton X-100 and 1× protease inhibitor cocktail) and sonicated for five cycles using Bioruptor (high power, 1 cycle = on for 30 s and off for 30 s). The sonicated sample was centrifuged at 15,000 rpm for 5 min, and supernatant transferred to a new tube was centrifuged at 15,000 rpm for 5 min. Sonicated chromatin was recovered and processed for immunoprecipitation of the chromatin. After saving 40 µl of chromatin as input, 10 µl of anti-FLAG–M2–agarose beads (A2220; Sigma-Aldrich) was added to 400 µl chromatin and incubated at 4 °C with rotation for 2 h. Beads were washed as described for the co-IP assays. Input chromatin and immunoprecipitated chromatin bound on beads were processed as described previously[48]. qPCR was performed as described above, and the relative enrichment was calculated by normalizing against ChIP–qPCR of non-transgenic control samples using *PP2A* (ref. 53). The normalized values of fold enrichment are the average ± s.e. of three biological replicates (two technical repeats each) from independent pools of tissues. Fold enrichment was calculated from each sample relative to the non-transgenic control (set as 1.0).

For the construction of the ChIP–seq library, transgenic *Arabidopsis* seedlings carrying P_{RGA}*:FLAG–RGA/rga-11* (in the *sly1 dP* background) and their respective control constructs without FLAG tags (*sly1 dQ* containing WT *RGA* and *sly1 dP*) were processed for ChIP as described above, except that chromatin was obtained after 25 cycles of sonication and 200 mg of starting ground powder and 20 µl of anti-FLAG–M2–agarose beads (A2220; Sigma-Aldrich) were used instead. Two biological repeats were prepared for each genotype.

Sequencing of the ChIP–seq library and data analyses

To prepare the ChIP–seq DNA library from purified DNA from ChIP, we followed the protocol published previously with minor modifications[53,73]. Two biological replicates of ChIP samples were pooled together for sequencing. We used the NEB's (http://www.neb.com) Y-adapter sequences and amplification primers sequences with

barcodes instead (Supplementary Table 9). DNA sequencing was performed using the Illumina platform.

After trimming adaptor sequences using Trimmomatic (v.0.39), paired-end ChIP–seq reads were mapped to the *Arabidopsis* reference genome (TAIR10) with Bowtie2 (v.2.4.5). Binding peaks were identified using MACS (v.2.2.7.1)[74] with default parameters except for '-f BAMPE' to model peaks from paired-end ChIP–seq data, comparing FLAG–RGA and FLAG–rga-11 to their respective controls without FLAG tags (*sdQ*) for FLAG–RGA, and *sdP* for FLAG–rga-11. After removing peaks from a small number of genomic regions where the mapped ChIP–seq read depths were consistently high across all samples including controls, we selected peaks with q values < 10^{-3}. Among them, we considered peaks with fold enrichment values higher than *GID1B* as high confidence because this gene had the lowest fold of enrichment in our dataset among all previously identified RGA target genes by ChIP–qPCR (Supplementary Table 2)[19–21,28,34,37,48,64,67]. The cumulative ratio of FLAG–RGA and FLAG–rga-11 read depth within 1.5 kb of all high-confidence peaks were visualized using deepTools (v.3.1.3). Following a previous study[20], we identified the set of all genes with a high-confidence FLAG–RGA peak within 5′ 3 kb and 3′ 1.5 kb using BEDtools (v.2.30.0) and made a comparison with the gene set with a GFP–rgaΔ17 peak[20]. To calculate the median ratio of ChIP to background read counts, deepTools was used to plot the ratio of FLAG–RGA to *sdQ* and FLAG–rga-11 to *sdP* to remove the background.

For the detection of RGA direct targets, we considered genes showing significant different (P < 0.001) expression between mock- and GA-treated samples in the *ga1* mutant plants, obtained from previous RNA-seq results[37], as putative DELLA-regulated genes because DELLA is known to be degraded by GA treatment[11]. Among the putative DELLA-regulated genes, those with a high-confidence FLAG–RGA peak within 5′ 3 kb and 3′ 1.5 kb were designated as RGA direct target genes. Gene Ontology enrichment analysis was done using GeneOntology (http://geneontology.org/).

TF-binding motifs enriched near peaks (within the region ±200 bp) of the peak centre were detected by the HOMER package v.4.11 (http://homer.ucsd.edu/homer/), using motif libraries derived from published DNA Affinity Purification (DAP)-seq and ChIP–seq data[75], and only displayed the motifs with $P \leq 0.01$. To calculate the motif enrichment from the overlap peaks between FLAG–RGA ChIP–seq and RNA-seq, the summit peak file was used to normalize the peak to be same ±200 bp size centred on the summit peak using HOMER package.

To calculate the genomic distribution of RGA binding peaks, the two R packages ChIPseeker (v.1.36.0) and GenomicFeatures (v.1.52.1) were used. The narrow peak files of FLAG–RGA or GFP–rgaΔ17 was used as the input file, and then we input the annotation file 'TAIR10_GFF3_genes_transposons.gff' (modified the file from TAIR database) and set the promoter region from −3 kb to 1 kb based on the TSS. The genome browser images were created using the Integrative Genomics Viewer 2.12.2.

Nuclei purification and ATAC-seq library preparation

Nuclei were purified using sucrose sedimentation as previously reported[76] with slight modifications as noted below. Ten-day-old seedlings grown in liquid culture (0.5× MS with 1% sucrose) were ground to fine powder in liquid nitrogen using a mortar and pestle. For each sample, 0.2 g of the frozen tissue powder was homogenized in prechilled 10 ml NPB buffer, and the nuclear fraction was purified as described[76]. The nuclei pellet was resuspended in 1 ml cold NPB buffer. For ATAC-seq, a 25 µl nuclei aliquot was stained with DAPI (0.2 µl, 1 µg per µl) and counted using a haemocytometer.

The ATAC assay was performed as previously described[77,78] with slight modifications. Approximately 50,000 nuclei were used for each ATAC-seq reaction. The purified nuclei were pelleted by swing bucket centrifugation at 1,500*g* for 7 min at 4 °C, and the supernatant was removed, leaving ~10 µl at the bottom of the tube. The Tn5 reaction was performed using a Tagment DNA Enzyme and Buffer kit (20034210; Illumina) as follows: 50 µl reaction mix containing 10 µl nuclei sample, 25 µl 2× TD buffer and 2 µl TDE1 was placed in an Applied Biosystems ProFlex thermocycler at 37 °C for 30 min. The tagmented DNA was purified using a MinElute PCR Purification kit (28004; QIAGEN) and eluted in 24 µl elution buffer. The purified tagmented DNA was first amplified using Next High-Fidelity 2× PCR Master Mix (M0541S; NEB) in 50 µl reactions, and a distinct barcoded primer 2 was used for each library (Supplementary Table 9). A 5 µl aliquot was removed from each reaction to be used for qPCR, using a LightCycler 96 instrument (Roche) to determine the number (n) of additional cycles needed to amplify the library. The remaining 45 µl of each PCR sample was then continued for an additional n cycles, and the resulting libraries were purified using AMPure beads (A63881; Beckman Coulter), eluting in 20 µl of elution buffer. Two biological repeats were performed for each sample. Each library was quantified using a Agilent 2100 Bioanalyzer before pooling for DNA sequencing (~11 ng per library) by the Illumina HiSeq 4000 (2× 150 bp paired end, ~40 million reads for each library).

Analysis of ATAC-seq data

We obtained around 20M paired-end reads for each independent biological replicate of the different genotypes. Quality trimming and adaptor removal were performed using Trim Galore v.0.6.4. The reads were mapped to the TAIR10 *Arabidopsis* reference genome using Bowtie2 v.2.4.5 (ref. 79). Subsequently, the organelle genomes were removed using samtools v.1.12[80]. PCR duplicates were discarded from the mapped reads using samblaster v.0.1.26 (ref. 81).

The regions with an artefactual massive amount of unique mapped reads were identified as a list of blacklisted genomic regions[57] and were removed from the mapped BAM files using samtools. The independent biological replicates were merged using samtools. Then, Tn5 hypersensitive sites were identified using MACS2 with the parameters: –nomodel –shift –100 –extsize 200 -q 0.05. The accessibility signals were normalized using the bamCoverage from deepTools v.3.5.1 (ref. 82). The normalized accessibility signals across whole *Arabidopsis* genome regions were generated using computeMatrix and plotProfile from deepTools. The DARs were identified using the R package DiffBind v.3.8.4 (ref. 83). The bw files were generated using the function bamCoverage from deepTools with CPM as normalization. The gene annotations were performed using BEDtools v.2.30.0 with the parameters: closest -D a -k 4. The metaplots were generated using the function plotProfile from deepTools. The genome browser images were created using the Integrative Genomics Viewer 2.12.2.

Comparison between FLAG–RGA binding peaks and published ChIP–seq datasets for PIF4, H2Aub1 and H2A.Z/H3

The ChIP–seq datasets were downloaded from the National Center for Biotechnology Information (PIF4, accession number GSM865710 (ref. 53); H2Aub1, accession number GSE155378 (ref. 57); and H2A.Z/H3, accession number GSE96873 (ref. 62)). Data analysis was the same as for ATAC-seq until the bam files with reads mapped to *Arabidopsis* genome were generated. The bw files were generated using the command bamCompare from deepTools with 'ratio' accounting for scaling. For H2A.Z/H3, the bam file with H3 coverage across genome was used as the control. The positional files, which contain the coordinates of overlapped genes between the peaks from RGA and that from the corresponding dataset, were generated using narrow peak files with both TSS and AGInames. The metaplots were generated using the commands computeMatrix and plotProfile from deepTools, with the bw files providing signal intensity while the positional files providing positional information.

Comparison between FLAG–RGA binding peaks and nucleosome profile

The nucleosome positioning in WT Col-0 seedlings was analysed using micrococcal nuclease sequencing dataset (PRJNA780072)[63,84]

by DANPOS v.2.2.2 (ref. 85). The dpos.py command of DANPOS was used to obtain the wigs file with normalized coverage of nucleosomes. Then, the wigs file was transformed into the bw file by the command wigToBigWig v.4. The metaplots of nucleosome positioning were generated by deepTools based on 2,228 genes that are associated with RGA binding peaks in our study.

Reporting summary

Further information on research design is available in the Nature Portfolio Reporting Summary linked to this article.

Data availability

Raw and processed ChIP–seq data and ATAC-seq data have been deposited at the National Center for Biotechnology Information's Gene Expression Omnibus (accession numbers GSE220898 and GSE233124, respectively). Source data are provided with this paper.

References

1. Peng, J. et al. 'Green revolution' genes encode mutant gibberellin response modulators. *Nature* **400**, 256–261 (1999).
2. Eshed, Y. & Lippman, Z. B. Revolutions in agriculture chart a course for targeted breeding of old and new crops. *Science* **366**, eaax0025 (2019).
3. Sun, T. P. The molecular mechanism and evolution of the GA-GID1-DELLA signaling module in plants. *Curr. Biol.* **21**, R338–R345 (2011).
4. Silverstone, A. L., Ciampaglio, C. N. & Sun, T.-P. The *Arabidopsis RGA* gene encodes a transcriptional regulator repressing the gibberellin signal transduction pathway. *Plant Cell* **10**, 155–169 (1998).
5. Peng, J. et al. The *Arabidopsis GAI* gene defines a signalling pathway that negatively regulates gibberellin responses. *Genes Dev.* **11**, 3194–3205 (1997).
6. Hernandez-Garcia, J., Briones-Moreno, A. & Blazquez, M. A. Origin and evolution of gibberellin signaling and metabolism in plants. *Semin. Cell Dev. Biol.* **109**, 46–54 (2021).
7. Daviere, J. M. & Achard, P. A pivotal role of DELLAs in regulating multiple hormone signals. *Mol. Plant* **9**, 10–20 (2016).
8. Van De Velde, K. et al. Exploiting DELLA signaling in cereals. *Trends Plant Sci.* **22**, 880–893 (2017).
9. Pysh, L. D. et al. The GRAS gene family in Arabidopsis: sequence characterization and basic expression analysis of the SCARECROW-LIKE genes. *Plant J.* **18**, 111–119 (1999).
10. Tian, C. et al. Genome-wide analysis of the GRAS gene family in rice and Arabidopsis. *Plant Mol. Biol.* **54**, 519–532 (2004).
11. Silverstone, A. L. et al. Repressing a repressor: gibberellin-induced rapid reduction of the RGA protein in *Arabidopsis*. *Plant Cell* **13**, 1555–1566 (2001).
12. Dill, A., Jung, H.-S. & Sun, T.-P. The DELLA motif is essential for gibberellin-induced degradation of RGA. *Proc. Natl Acad. Sci. USA* **98**, 14162–14167 (2001).
13. Ueguchi-Tanaka, M. et al. *GIBBERELLIN INSENSITIVE DWARF1* encodes a soluble receptor for gibberellin. *Nature* **437**, 693–698 (2005).
14. Griffiths, J. et al. Genetic characterization and functional analysis of the GID1 gibberellin receptors in *Arabidopsis*. *Plant Cell* **18**, 3399–3414 (2006).
15. Sasaki, A. et al. Accumulation of phosphorylated repressor for gibberellin signaling in an F-box mutant. *Science* **299**, 1896–1898 (2003).
16. McGinnis, K. M. et al. The *Arabidopsis SLEEPY1* gene encodes a putative F-box subunit of an SCF E3 ubiquitin ligase. *Plant Cell* **15**, 1120–1130 (2003).
17. Murase, K., Hirano, Y., Sun, T.-P. & Hakoshima, T. Gibberellin-induced DELLA recognition by the gibberellin receptor GID1. *Nature* **456**, 459–463 (2008).
18. Shimada, A. et al. Structural basis for gibberellin recognition by its receptor GID1. *Nature* **456**, 520–523 (2008).
19. Zentella, R. et al. Global analysis of DELLA direct targets in early gibberellin signaling in *Arabidopsis*. *Plant Cell* **19**, 3037–3057 (2007).
20. Serrano-Mislata, A. et al. DELLA genes restrict inflorescence meristem function independently of plant height. *Nat. Plants* **3**, 749–754 (2017).
21. Marin-de la Rosa, N. et al. Genome wide binding site analysis reveals transcriptional coactivation of cytokinin-responsive genes by DELLA proteins. *PLoS Genet.* **11**, e1005337 (2015).
22. Marin-de la Rosa, N. et al. Large-scale identification of gibberellin-related transcription factors defines group VII ETHYLENE RESPONSE FACTORS as functional DELLA partners. *Plant Physiol.* **166**, 1022–1032 (2014).
23. Lantzouni, O. et al. GROWTH-REGULATING FACTORS interact with DELLAs and regulate growth in cold stress. *Plant Cell* **32**, 1018–1034 (2020).
24. Feng, S. et al. Coordinated regulation of *Arabidopsis thaliana* development by light and gibberellins. *Nature* **451**, 475–479 (2008).
25. de Lucas, M. et al. A molecular framework for light and gibberellin control of cell elongation. *Nature* **451**, 480–484 (2008).
26. Oh, E. et al. Cell elongation is regulated through a central circuit of interacting transcription factors in the *Arabidopsis* hypocotyl. *eLife* **3**, e03031 (2014).
27. Hu, J., Israeli, A., Ori, N. & Sun, T. P. The interaction between DELLA and ARF/IAA mediates crosstalk between gibberellin and auxin signaling to control fruit initiation in tomato. *Plant Cell* **30**, 1710–1728 (2018).
28. Bai, M. Y. et al. Brassinosteroid, gibberellin, and phytochrome signalling pathways impinge on a common transcription module in *Arabidopsis*. *Nat. Cell Biol.* **14**, 810–817 (2012).
29. Hou, X. et al. DELLAs modulate jasmonate signaling via competitive binding to JAZs. *Dev. Cell* **19**, 884–894 (2010).
30. Yang, D. L. et al. Plant hormone jasmonate prioritizes defense over growth by interfering with gibberellin signaling cascade. *Proc. Natl Acad. Sci. USA* **109**, E1192–E1200 (2012).
31. Daviere, J. M. et al. Class I TCP-DELLA interactions in inflorescence shoot apex determine plant height. *Curr. Biol.* **24**, 1923–1928 (2014).
32. Lim, S. et al. ABA-insensitive3, ABA-insensitive5, and DELLAs Interact to activate the expression of SOMNUS and other high-temperature-inducible genes in imbibed seeds in *Arabidopsis*. *Plant Cell* **25**, 4863–4878 (2013).
33. Yoshida, H. et al. DELLA protein functions as a transcriptional activator through the DNA binding of the INDETERMINATE DOMAIN family proteins. *Proc. Natl Acad. Sci. USA* **111**, 7861–7866 (2014).
34. Fukazawa, J. et al. DELLAs function as coactivators of GAI-ASSOCIATED FACTOR1 in regulation of gibberellin homeostasis and signaling in *Arabidopsis*. *Plant Cell* **26**, 2920–2938 (2014).
35. Sarnowska, E. A. et al. DELLA-interacting SWI3C core subunit of switch/sucrose nonfermenting chromatin remodeling complex modulates gibberellin responses and hormonal cross talk in *Arabidopsis*. *Plant Physiol.* **163**, 305–317 (2013).
36. Zhang, D., Jing, Y., Jiang, Z. & Lin, R. The chromatin-remodeling factor PICKLE integrates brassinosteroid and gibberellin signaling during skotomorphogenic growth in *Arabidopsis*. *Plant Cell* **26**, 2472–2485 (2014).
37. Park, J. et al. GA signaling requires chromatin remodeler PICKLE to promote vegetative growth and phase transitions. *Plant Physiol.* **173**, 1463–1474 (2017).
38. Locascio, A., Blazquez, M. A. & Alabadi, D. Dynamic regulation of cortical microtubule organization through prefoldin-DELLA interaction. *Curr. Biol.* **23**, 804–809 (2013).

39. Dill, A., Thomas, S. G., Hu, J., Steber, C. M. & Sun, T.-P. The *Arabidopsis* F-box protein SLEEPY1 targets GA signaling repressors for GA-induced degradation. *Plant Cell* **16**, 1392–1405 (2004).
40. Chandler, P. M. & Harding, C. A. 'Overgrowth' mutants in barley and wheat: new alleles and phenotypes of the 'green revolution' DELLA gene. *J. Exp. Bot.* **64**, 1603–1613 (2013).
41. Hirano, K. et al. The suppressive function of the rice DELLA protein SLR1 is dependent on its transcriptional activation activity. *Plant J.* **71**, 443–453 (2012).
42. Ikeda, A. et al. *slender* rice, a constitutive gibberellin response mutant is caused by a null mutation of the *SLR1* gene, an ortholog of the height-regulating gene *GAI/RGA/RHT/D8*. *Plant Cell* **13**, 999–1010 (2001).
43. Muangprom, A., Thomas, S. G., Sun, T. P. & Osborn, T. C. A novel dwarfing mutation in a green revolution gene from *Brassica rapa*. *Plant Physiol.* **137**, 931–938 (2005).
44. Hirano, K. et al. Characterization of the molecular mechanism underlying gibberellin perception complex formation in rice. *Plant Cell* **22**, 2680–2696 (2010).
45. Zentella, R. et al. *O*-GlcNAcylation of master growth repressor DELLA by SECRET AGENT modulates multiple signaling pathways in *Arabidopsis*. *Genes Dev.* **30**, 164–176 (2016).
46. Silverstone, A. L., Mak, P. Y. A., Casamitjana Martínez, E. & Sun, T.-P. The new *RGA* locus encodes a negative regulator of gibberellin response in *Arabidopsis thaliana*. *Genetics* **146**, 1087–1099 (1997).
47. Matsuo, N., Minami, M., Maeda, T. & Hiratsuka, K. Dual luciferase assay for monitoring transient gene expression in higher plants. *Plant Biotechnol.* **18**, 71–75 (2001).
48. Zhang, Z. L. et al. SCARECROW-LIKE 3 promotes gibberellin signaling by antagonizing DELLA in *Arabidopsis*. *Proc. Natl Acad. Sci. USA* **108**, 2160–2165 (2011).
49. Hirano, Y. et al. Structure of the SHR-SCR heterodimer bound to the BIRD/IDD transcriptional factor JKD. *Nat. Plants* **3**, 17010 (2017).
50. Arnold, K., Bordoli, L., Kopp, J. & Schwede, T. The SWISS-MODEL workspace: a web-based environment for protein structure homology modelling. *Bioinformatics* **22**, 195–201 (2006).
51. Dill, A. & Sun, T.-P. Synergistic de-repression of gibberellin signaling by removing RGA and GAI function in *Arabidopsis thaliana*. *Genetics* **159**, 777–785 (2001).
52. King, K., Moritz, T. & Harberd, N. Gibberellins are not required for normal stem growth in *Arabidopsis thaliana* in the absence of GAI and RGA. *Genetics* **159**, 767–776 (2001).
53. Oh, E., Zhu, J. Y. & Wang, Z. Y. Interaction between BZR1 and PIF4 integrates brassinosteroid and environmental responses. *Nat. Cell Biol.* **14**, 802–809 (2012).
54. Barbour, H., Daou, S., Hendzel, M. & Affar, E. B. Polycomb group-mediated histone H2A monoubiquitination in epigenome regulation and nuclear processes. *Nat. Commun.* **11**, 5947 (2020).
55. Colino-Sanguino, Y., Clark, S. J. & Valdes-Mora, F. The H2A.Z-nuclesome code in mammals: emerging functions. *Trends Genet.* **38**, 273–289 (2022).
56. Long, J., Carter, B., Johnson, E. T. & Ogas, J. Contribution of the histone variant H2A.Z to expression of responsive genes in plants. *Semin. Cell Dev. Biol.* **135**, 85–92 (2023).
57. Yin, X. et al. H2AK121ub in *Arabidopsis* associates with a less accessible chromatin state at transcriptional regulation hotspots. *Nat. Commun.* **12**, 315 (2021).
58. Zhou, Y., Romero-Campero, F. J., Gomez-Zambrano, A., Turck, F. & Calonje, M. H2A monoubiquitination in *Arabidopsis thaliana* is generally independent of LHP1 and PRC2 activity. *Genome Biol.* **18**, 69 (2017).
59. Lei, B. & Berger, F. H2A variants in *Arabidopsis*: versatile regulators of genome activity. *Plant Commun.* **1**, 100015 (2020).
60. Sura, W. et al. Dual role of the histone variant H2A.Z in transcriptional regulation of stress-response genes. *Plant Cell* **29**, 791–807 (2017).
61. Gomez-Zambrano, A., Merini, W. & Calonje, M. The repressive role of *Arabidopsis* H2A.Z in transcriptional regulation depends on AtBMI1 activity. *Nat. Commun.* **10**, 2828 (2019).
62. Wollmann, H. et al. The histone H3 variant H3.3 regulates gene body DNA methylation in *Arabidopsis thaliana*. *Genome Biol.* **18**, 94 (2017).
63. Yang, T. et al. Chromatin remodeling complexes regulate genome architecture in *Arabidopsis*. *Plant Cell* **34**, 2638–2651 (2022).
64. Yamaguchi, N. et al. Gibberellin acts positively then negatively to control onset of flower formation in *Arabidopsis*. *Science* **344**, 638–641 (2014).
65. Jin, R. et al. LEAFY is a pioneer transcription factor and licenses cell reprogramming to floral fate. *Nat. Commun.* **12**, 626 (2021).
66. Tyler, L. et al. DELLA proteins and gibberellin-regulated seed germination and floral development in *Arabidopsis*. *Plant Physiol.* **135**, 1008–1019 (2004).
67. Park, J., Nguyen, K. T., Park, E., Jeon, J. S. & Choi, G. DELLA proteins and their interacting RING finger proteins repress gibberellin responses by binding to the promoters of a subset of gibberellin-responsive genes in *Arabidopsis*. *Plant Cell* **25**, 927–943 (2013).
68. Steber, C. M. & McCourt, P. A role for brassinosteroids in germination in *Arabidopsis thaliana*. *Plant Physiol.* **125**, 763–769 (2000).
69. Zentella, R. et al. The *Arabidopsis O*-fucosyltransferase SPINDLY activates nuclear growth repressor DELLA. *Nat. Chem. Biol.* **13**, 479–485 (2017).
70. Zentella, R. et al. SPINDLY *O*-fucosylates nuclear and cytoplasmic proteins involved in diverse cellular processes in plants. *Plant Physiol.* **191**, 1546–1560 (2023).
71. Biasini, M. et al. SWISS-MODEL: modelling protein tertiary and quaternary structure using evolutionary information. *Nucleic Acids Res.* **42**, W252–W258 (2014).
72. Zhou, X. et al. The ERF11 transcription factor promotes internode elongation by activating gibberellin biosynthesis and signaling. *Plant Physiol.* **171**, 2760–2770 (2016).
73. Wong, K. H., Jin, Y. & Moqtaderi, Z. Multiplex Illumina sequencing using DNA barcoding. *Curr. Protoc. Mol. Biol.* **7**, 7.11.11–17.11.11 (2013).
74. Feng, J., Liu, T., Qin, B., Zhang, Y. & Liu, X. S. Identifying ChIP–seq enrichment using MACS. *Nat. Protoc.* **7**, 1728–1740 (2012).
75. O'Malley, R. C. et al. Cistrome and epicistrome features shape the regulatory DNA landscape. *Cell* **165**, 1280–1292 (2016).
76. Bajic, M., Maher, K. A. & Deal, R. B. Identification of open chromatin regions in plant genomes using ATAC-seq. *Methods Mol. Biol.* **1675**, 183–201 (2018).
77. Buenrostro, J. D., Wu, B., Chang, H. Y. & Greenleaf, W. J. ATAC-seq: a method for assaying chromatin accessibility genome-wide. *Curr. Protoc. Mol. Biol.* **109**, 21.29.21–21.29.29 (2015).
78. Potter, K. C., Wang, J., Schaller, G. E. & Kieber, J. J. Cytokinin modulates context-dependent chromatin accessibility through the type-B response regulators. *Nat. Plants* **4**, 1102–1111 (2018).
79. Langmead, B. & Salzberg, S. L. Fast gapped-read alignment with Bowtie 2. *Nat. Methods* **9**, 357–359 (2012).
80. Danecek, P. et al. Twelve years of SAMtools and BCFtools. *Gigascience* **10**, giab008 (2021).
81. Faust, G. G. & Hall, I. M. SAMBLASTER: fast duplicate marking and structural variant read extraction. *Bioinformatics* **30**, 2503–2505 (2014).

82. Ramirez, F. et al. deepTools2: a next generation web server for deep-sequencing data analysis. *Nucleic Acids Res.* **44**, W160–W165 (2016).
83. Ross-Innes, C. S. et al. Differential oestrogen receptor binding is associated with clinical outcome in breast cancer. *Nature* **481**, 389–393 (2012).
84. Diego-Martin, B. et al. The TRIPLE PHD FINGERS proteins are required for SWI/SNF complex-mediated +1 nucleosome positioning and transcription start site determination in *Arabidopsis*. *Nucleic Acids Res.* **50**, 10399–10417 (2022).
85. Chen, K. et al. DANPOS: dynamic analysis of nucleosome position and occupancy by sequencing. *Genome Res* **23**, 341–351 (2013).

Acknowledgements

We thank G. Choi for helpful discussions and for sharing *Arabidopsis* lines and constructs. This work was supported by the National Institutes of Health (R01 GM100051 to T.-P.S.) and the National Science Foundation (MCB-1818161 to T.-P.S., and NSF-EDGE-1923589 to D.-H.O. and M.D.). We also acknowledge Louisiana State University High Performance Computing services for providing computational resources.

Author contributions

J.P. and T.-P.S. conceived and designed the research project. R.Z. provided helpful suggestions. H.Q. provided constructs and protocols. X.H., H.T., J.P., J.H. and R.Z. performed experiments. X.H., H.T., J.P., J.H., R.Z. and T.-P.S. analysed the data and generated figures. D.-H.O., J.P., H.T. and M.D. performed analysis for the ChIP–seq data and generated figures. T.-P.S. wrote the paper with input from all co-authors.

Competing interests

The authors declare no competing interests.

Additional information

Supplementary information The online version contains supplementary material available at https://doi.org/10.1038/s41477-023-01477-y.

Correspondence and requests for materials should be addressed to Tai-Ping Sun.

Peer review information *Nature Plants* thanks the anonymous reviewers for their contribution to the peer review of this work.

nature portfolio

Corresponding author(s): Tai-ping Sun

Last updated by author(s): 2023/06/29

Reporting Summary

Nature Portfolio wishes to improve the reproducibility of the work that we publish. This form provides structure for consistency and transparency in reporting. For further information on Nature Portfolio policies, see our Editorial Policies and the Editorial Policy Checklist.

Statistics

For all statistical analyses, confirm that the following items are present in the figure legend, table legend, main text, or Methods section.

n/a	Confirmed
☐	☒ The exact sample size (*n*) for each experimental group/condition, given as a discrete number and unit of measurement
☐	☒ A statement on whether measurements were taken from distinct samples or whether the same sample was measured repeatedly
☐	☒ The statistical test(s) used AND whether they are one- or two-sided *Only common tests should be described solely by name; describe more complex techniques in the Methods section.*
☒	☐ A description of all covariates tested
☒	☐ A description of any assumptions or corrections, such as tests of normality and adjustment for multiple comparisons
☐	☒ A full description of the statistical parameters including central tendency (e.g. means) or other basic estimates (e.g. regression coefficient) AND variation (e.g. standard deviation) or associated estimates of uncertainty (e.g. confidence intervals)
☐	☒ For null hypothesis testing, the test statistic (e.g. *F*, *t*, *r*) with confidence intervals, effect sizes, degrees of freedom and *P* value noted *Give P values as exact values whenever suitable.*
☒	☐ For Bayesian analysis, information on the choice of priors and Markov chain Monte Carlo settings
☒	☐ For hierarchical and complex designs, identification of the appropriate level for tests and full reporting of outcomes
☒	☐ Estimates of effect sizes (e.g. Cohen's *d*, Pearson's *r*), indicating how they were calculated

Our web collection on statistics for biologists contains articles on many of the points above.

Software and code

Policy information about availability of computer code

Data collection	Microsoft 365 Apps for Enterprise
Data analysis	Microsoft 365 Apps for Enterprise; MACS (v.2.2.7.1), Bowtie2 (v.2.4.5), BEDtools (v.2.30.0), DeepTools (v3.1.3), HOMER package (v4.11), ChIPseeker (v1.36.0), GenomicFeatures (v1.52.1), Trim Galore v0.6.4, samtools v1.12, samblaster v0.1.26, DANPOS v2.2.2, Pymol package v2.1.1.

For manuscripts utilizing custom algorithms or software that are central to the research but not yet described in published literature, software must be made available to editors and reviewers. We strongly encourage code deposition in a community repository (e.g. GitHub). See the Nature Portfolio guidelines for submitting code & software for further information.

Data

Policy information about availability of data

All manuscripts must include a data availability statement. This statement should provide the following information, where applicable:

- Accession codes, unique identifiers, or web links for publicly available datasets
- A description of any restrictions on data availability
- For clinical datasets or third party data, please ensure that the statement adheres to our policy

The ChIP-Seq and ATAC-seq data are available at NCBI's Gene Expression Omnibus (GSE220898 and GSE233124). Other raw quantitative data will be included as Source Data files and Supplementary Data.

Field-specific reporting

Please select the one below that is the best fit for your research. If you are not sure, read the appropriate sections before making your selection.

☒ Life sciences ☐ Behavioural & social sciences ☐ Ecological, evolutionary & environmental sciences

For a reference copy of the document with all sections, see nature.com/documents/nr-reporting-summary-flat.pdf

Life sciences study design

All studies must disclose on these points even when the disclosure is negative.

Sample size	Sample size for measuring plant heights was 8-12, and for hypocotyl lengths was 13-14. Sample size was determined based on the reproducibility of each experiment. Exact n values are listed in Source Data files.
Data exclusions	No data were excluded from analysis.
Replication	Phenotype analysis, pulldown and co-IP were repeated two or three times as specified in figure legends. ChIP-Seq was performed using two biological replicas for ChIP. ATAC-seq was performed using two biological replicas. All other experiments were performed using three biological repeats. Similar results were confirmed in all replications of each experiment and representative data were shown. In all experiments, all attempts at replication were successful.
Randomization	Sample allocation was random.
Blinding	Specific genotypes or protein combinations are needed for different assays, and this makes it impossible to conduct blinding assays.

Reporting for specific materials, systems and methods

We require information from authors about some types of materials, experimental systems and methods used in many studies. Here, indicate whether each material, system or method listed is relevant to your study. If you are not sure if a list item applies to your research, read the appropriate section before selecting a response.

Materials & experimental systems

n/a	Involved in the study
☐	☒ Antibodies
☒	☐ Eukaryotic cell lines
☒	☐ Palaeontology and archaeology
☒	☐ Animals and other organisms
☒	☐ Human research participants
☒	☐ Clinical data
☒	☐ Dual use research of concern

Methods

n/a	Involved in the study
☐	☒ ChIP-seq
☒	☐ Flow cytometry
☒	☐ MRI-based neuroimaging

Antibodies

Antibodies used	HRP anti-FLAG M2 mouse monoclonal (Sigma Aldrich A8592, , lot #109M4793V), anti-HA.11 mouse monoclonal (BioLegend 901503, clone 16B12, lot #B326653), HRP anti-c-Myc mouse monoclonal antibody (BioLegend 626803, clone 9E10, lot #B373346), anti-H2A rabbit monoclonal antibody (Abcam#ab177308, clone EPR17470, lot #GR221838-9) and anti-Histone 3 rabbit polyclonal antibody (Abcam ab1791), anti-RGA rabbit polyclonal antibody (DU176, generated by our lab), anti-c-Myc agarose (Sigma-Aldrich A7470, lot # 0000135031, rabbit polyclonal), anti-FLAG M2 agarose (Sigma-Aldrich A2220, lot #SLCH0130), HRP-conjugated donkey anti-mouse IgG (Jackson ImmunoResearch #715-035-150, lot #144459), HRP-conjugated goat anti-rabbit IgG (Thermo-Fisher #31462, lot #GF953108).
Validation	Sigma A8592 has minimum detection of 8 ng of FLAG-fusion protein (sigmaaldrich.com), and was validated by previous papers of our lab; Biolegend 901503 (anti-HA.11) was quality control tested by western blotting. The HA.11 antibody recognizes HA epitopes located in the middle of protein sequences as well as at the N- or C-terminus. Anti-H2A antibody (Abcam #ab177308) was validated by GST or GST-H2A protein blot. Anti-Histone 3 antibody (Abcam #ab1791) reacts with H3 variants in multiple species including Arabidopsis thaliana. Anti-RGA antiserum (DU176) was validated by previous papers of our lab using recombinant RGA and transgenic lines expressing GFP-RGA fusion. In all our experiments, we included the non-transgenic parental line as the negative control.

ChIP-seq

Data deposition

☒ Confirm that both raw and final processed data have been deposited in a public database such as GEO.

☒ Confirm that you have deposited or provided access to graph files (e.g. BED files) for the called peaks.

Data access links *May remain private before publication.*	GSE220898 for accessing our data at NCBI GEO is available to the public.
Files in database submission	220214_PE_FRGA_vs_RGA_sly1_dQ_rmdup_q5E-2q1E-3_summits.cleaned.long.bed, 220214_PE_Frga11_vs_sly1_dQ_rmdup_q5E-2q1E-3_summits.cleaned.long.bed 220214_PE_FRGA_vs_RGA_sly1_dQ_rmdup_q5E-2q1E-3_peaks.cleaned.narrowPeak, 220214_PE_Frga11_vs_sly1_dQ_rmdup_q5E-2q1E-3_peaks.cleaned.narrowPeak, Codes_used_for_RGA_ChIPseq, Metadata spreadsheet-FRGA ChIP-seq FRGA-I4_R1_001.trimmed.paired.fq.gz, FRGA-I4_R2_001.trimmed.paired.fq.gz, Frga11-I10_S1_R1_001.trimmed.paired.fq.gz, Frga11-I10_S1_R2_001.trimmed.paired.fq.gz, RGA_sly1_dQ-I2_R1_001.trimmed.paired.fq.gz, RGA_sly1_dQ-I2_R2_001.trimmed.paired.fq.gz, sly1_dP-I7_R1_001.trimmed.paired.fq.gz, sly1_dP-I7_R2_001.trimmed.paired.fq.gz.
Genome browser session (e.g. UCSC)	no longer applicable

Methodology

Replicates	Two biological repeats per genotype for ChIP, and pooled ChIP DNA together for making the DNA library for sequencing as described previously (Oh et al. Nat Cell Biol (2012)).
Sequencing depth	FRGA sly1 dP, 34659562 (54.87%) of total 63162403, Frga11 sly1 dP, 41437867 (52.93%) of total 78291652, RGA sly1 dQ, 37399338 (53.15%) of total 70359479, sly1 dQ, 17023011 (40.62%) of total 41910879 read pairs were uniquely and concordantly mapped to the Arabidopsis TAIR10 nuclear genome sequences. All reads in pairs (paired-end) were minimum 50-nt long after trimming adaptor sequences.
Antibodies	anti-FLAG M2-Agarose (Sigma A2220)
Peak calling parameters	Binding peaks were identified using MACS (v.2.2.7.1) with default parameters except for '-f BAMPE' to model peaks from paired-ends ChIP-seq data, comparing FLAG-RGA and FLAG-(rga-11) to their respective controls without FLAG tags (RGA sly1 dQ for FLAG-RGA, and sly1 dP for FLAG-(rga-11)).
Data quality	We confirmed ChIP-seq results by ChIP-qPCR for 6 target peaks using 3 biological replicas.
Software	Trimmomatic v0.39, Bowtie2 (v.2.4.5), MACS (v.2.2.7.1), Deeptools (v. 3.1.3), Bedtools (v.2.30.0).